Precambrian Research 362 (2021) 106287

Contents lists available at ScienceDirect

Precambrian Research

journal homepage: www.elsevier.com/locate/precamres

The cause for Nuna breakup in the Early to Middle Mesoproterozoic

Zongying Huang [a,b], Chao Yuan [a,b,*], Xiaoping Long [c], Yunying Zhang [a], Xiaolong Ma [d], Jérémie Soldner [a,b], Long Du [e], Chutian Shu [f]

[a] State Key Laboratory of Isotope Geochemistry, Guangzhou Institute of Geochemistry, Chinese Academy of Sciences, Guangzhou 510640, China
[b] CAS Center for Excellence in Deep Earth Science, Guangzhou 510640, China
[c] State Key Laboratory of Continental Dynamics, Department of Geology, Northwest University, Northern Taibai Str. 229, Xi'an 710069, China
[d] Research School of Earth Sciences, The Australian National University, 142 Mills Road, Canberra, ACT 2601, Australia
[e] College of Geological Science and Engineering, Shandong University of Science and Technology, Qingdao 266590, China
[f] RC Centre of Excellence for Core to Crust Fluid Systems and Department of Earth and Environmental Sciences, Macquarie University, Sydney, New South Wales, Australia

A R T I C L E I N F O

Keywords:
Nuna Breakup
Subduction
Plume
Chinese Central Tianshan Block
Mesoproterozoic

A B S T R A C T

The dynamic mechanism responsible for the breakup of Nuna supercontinent (1.6–1.3 Ga) is a key for understanding the early to middle Mesoproterozoic environment, life and mineralization on Earth. Although much research has been done to unravel the dispersion of young supercontinents (e.g., Pangea), efforts by sorting out critical geological records to disclose the driving force for Nuna breakup are still rare. Here we focus on this issue by integrating new whole-rock geochemical data, zircon U–Pb ages, Hf-in-zircon and Nd isotopes for Mesoproterozoic granitoids in the Chinese Central Tianshan (CTB) at the Central Asian Orogenic Belt (CAOB). Moreover, global geological data in the early to middle Mesoproterozoic are compiled to place further constraints. The studied granitoids are I-type granites emplaced at ca. 1480–1450 Ma. They were formed in an active continental margin of CTB that once belonged to the Fennoscandia in the margin of Nuna. These results, together with the available geological records in CTB, CAOB and Fennoscandia, indicate a subduction system existed along the periphery of these domains in the early to middle Mesoproterozoic. This subduction system was temporally and spatially linked to the 1.6–1.3 Ga accretionary belts in the peripheral blocks of Nuna supercontinent, suggesting an encircling subduction system surrounding Nuna supercontinent. The encircling subduction system was accompanied by intermittent Mesoproterozoic plume magmatism, some of which were geochemically overprinted with subduction-related signatures, suggesting a dominant continuous circum-supercontinent subduction operating on the breakup of Nuna supercontinent. Moreover, these episodic plume-related magmatism are temporally and geodynamically linked to the exterior subduction surrounding the Nuna supercontinent. Our study therefore demonstrates that the development of an exterior subduction system gave rise to the breakup of Nuna supercontinent, which was accompanied by subordinate plume activities.

1. Introduction

The early to middle Mesoproterozoic has long been believed to be a enigmatic period (1.6–1.3 Ga) characterized by environmental stasis with tectonic stability (Buick et al., 1995; Brasier and Lindsay, 1998; Holland, 2006; Lyons et al., 2014), presenting with the paucity of banded iron formations, phosphorites, glaciation events and orogenic ore deposits related to the convergent systems (Goldfarb et al., 2001; Holland, 2006; Cawood and Hawkesworth, 2014; Mukherjee et al., 2018). Yet, this period does not seem to be static, as it involved the lifespan over the Nuna (or Columbia) supercontinent breakup. Nuna has been suggested to break up around 1.6–1.3 Ga (Zhao et al., 2004; Hou et al., 2008; Evans and Mitchell, 2011; Pisarevsky et al., 2014a, 2014b; Nordsvan et al., 2018; Pourteau et al., 2018). Recently, studies showed that oxygenation in this period was far more dynamic and intense than previously envisaged (Large et al., 2017; Zhang et al., 2018a). Revealing the dynamic mechanism for Nuna breakup is thus essential to understand the early to middle Mesoproterozoic enigmatic period, and has important significance for understanding the global environmental effect (e.g., atmospheric oxygen concentrations, ocean redox conditions)

* Corresponding author at: State Key Laboratory of Isotope Geochemistry, Guangzhou Institute of Geochemistry, Chinese Academy of Sciences, Guangzhou 510640, China.

E-mail address: yuanchao@gig.ac.cn (C. Yuan).

https://doi.org/10.1016/j.precamres.2021.106287
Received 26 February 2021; Received in revised form 26 May 2021; Accepted 26 May 2021
Available online 17 June 2021

and deposit formation in this period (Cawood and Hawkesworth, 2015; Pehrsson et al., 2016; Zhang et al., 2018a).

Although the breakup of Nuna might bring about profound impact on the environment and mineralization of the planet, how the supercontinent got into breakup is not yet fully understood. Previous studies mainly centered on post-Nuna supercontinents (e.g., Rodinia and Pangea) or relied on numerical modeling results. Conjectures involving subduction (e.g., Murphy and Nance, 2013; Bercovici and Long, 2014; Cawood et al., 2016; Dal Zilio et al., 2018; Niu, 2019) or/and superplume events have been proposed to be the dominant mechanisms for dispersal of the supercontinent (e.g., Hou et al., 2008; Li and Zhong, 2009; Santosh et al., 2009; Yoshida and Santosh, 2011; Burov and Gerya, 2014; Zhang et al., 2018b; Lu et al., 2020). No consensus has so far been achieved. Because most oceanic lithosphere and oceanic plume records in the period of Nuna breakup have been destroyed through subduction (Bradley, 2011; Doucet et al., 2019; Li, 2020), it is thus a challenging task to uncover the link between subduction/plume and Nuna breakup. Moreover, because most cratons or blocks of Nuna generally experienced multiple tectonic movements, many early geological records of Nuna were partly fragmented or even entirely erased in subsequent tectonothermal events. This makes investigating the role of subduction and plume on the breakup of Nuna difficult.

Breakup of a supercontinent is always accompanied with intense magmatism, and subduction-related and plume-related magmatism are two end members with strikingly different geological and geochemical characteristics. Clearly, discriminating the geological and geochemical features between subduction and plume allows for a better understanding of the dynamic regime of Nuna breakup. Subduction has been efficient in building island arcs along convergent margins with products of ophiolites, island-arc basalts (IAB), sheeted mafic dykes and

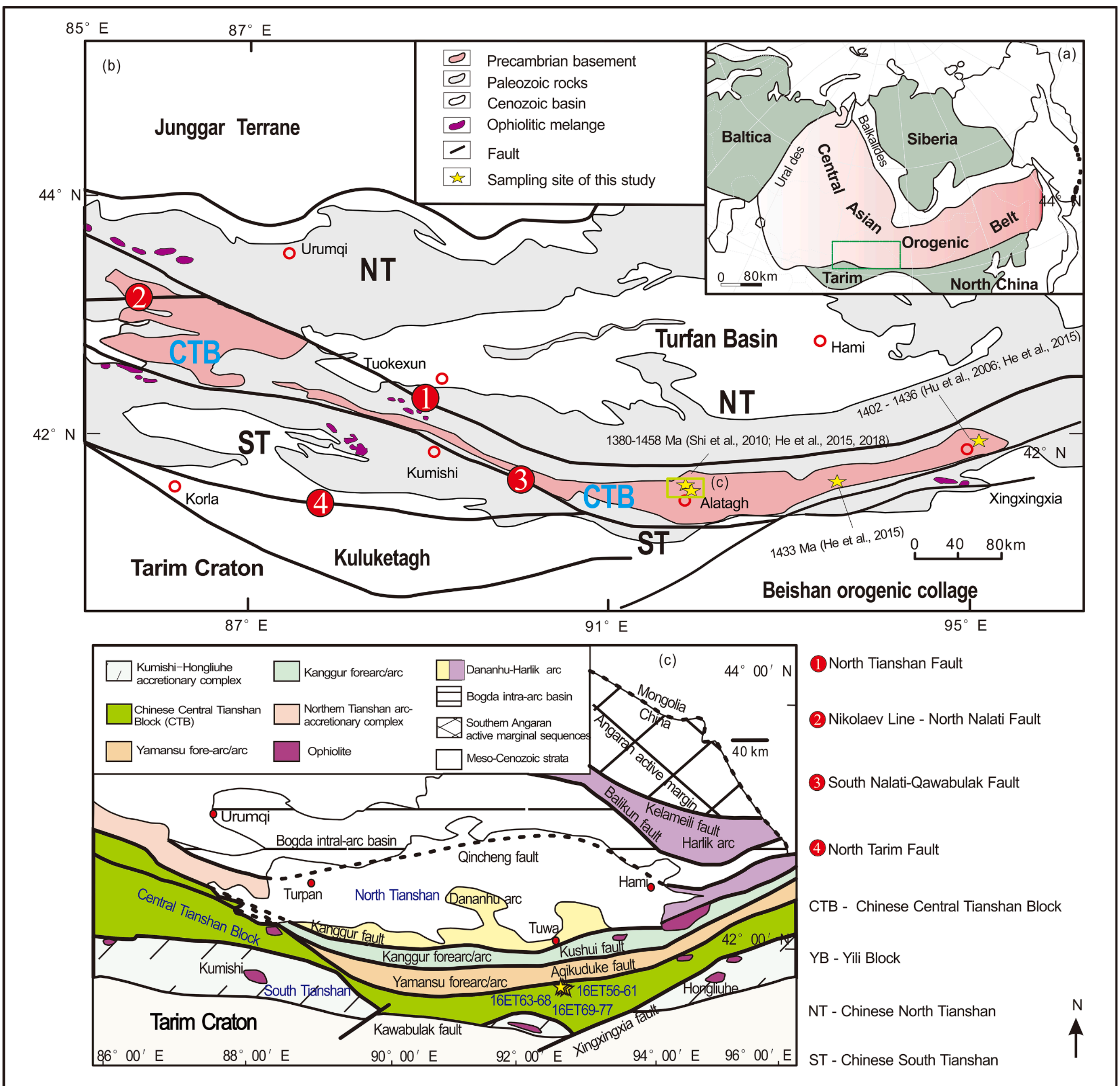

Fig. 1. (a) A simplified map of the Central Asian Orogenic Belt (after Jahn et al., 2000). (b) Sketch map of the Chinese Tianshan (after Huang et al., 2019). (c) Sketch map of the Chinese Central Tianshan (after Xiao et al., 2004).

granitoids (Tatsumi and Eggins, 1995; Stern, 2002; Dilek and Furnes, 2011). These subduction-derived rocks are usually produced in a water-rich and low temperature environment (Peacock, 1996; Stern, 2002; Grove et al., 2012). In subduction zones, two kinds of metamorphic conditions are present, namely high temperature-low pressure (HT-LP) and high pressure-low temperature (HP-LT) conditions. The first is produced due to heat input from arc magmatism, while the latter results from subduction of an oceanic slab (Banno et al., 1978; Brown, 1998; Ernst, 2005). By contrast, plume is capable of generating widespread massive magmatism, i.e., large igneous provinces that are commonly composed of mafic to ultra-mafic rocks, radial mafic dykes and within-plate granitoids (Morgan, 1971; White and McKenzie, 1989; Richards et al., 1991; Campbell, 2007; Ernst et al., 2008; Moucha and Forte, 2011). These plume-related magmas generally have higher temperature (up to 1550 °C) than subduction-related products (White and McKenzie, 1989; Xu et al., 2001; Herzberg and O'Hara, 2002; Mckenzie et al., 2005; Putirka et al., 2007; Brandl et al., 2013; Liu et al., 2014a). The high thermal anomaly introduced by the hot basaltic magma leads to widespread crustal melting and regional extension of the lithosphere (Hill, 1991; Campbell, 2001; Li et al., 2003).

Accretionary orogens and associated blocks record abundant information about the subduction and plume, and thus are essential for studying the supercontinent breakup. The Central Asian Orogenic belt, the largest accretionary orogen in the Phanerozoic, is thus undoubtedly the area where we can explore the cause for Nuna's fragmentation. Located in the southern Central Asian Orogenic Belt (CAOB) (Fig. 1a and 1b), the Chinese Central Tianshan Block (CTB) shares an affinity to Fennoscandia, located in the periphery of the Nuna (Huang et al., 2019). The well-preserved Mesoproterozoic records in both CTB and Fennoscandia (Ernst et al., 2008; Roberts and Slagstad, 2015; He et al., 2018; Huang et al., 2019) make them unique to investigate the breakup of Nuna. In this paper, we present new whole-rock geochemical data, zircon U–Pb ages, Hf-in-zircon and Nd isotope data for Mesoproterozoic granitoids in the CTB, aiming to reveal the dynamic mechanism for Nuna's breakup. In combination with available early to middle Mesoproterozoic data from Fennoscandia and associated blocks worldwide, we demonstrate that Nuna's breakup can be attributed to a circum-supercontinent subduction system with subordinate intermittent plume-related magmatism. The joint process was probably responsible for the oscillatory increase of oxygen level and complex of eukaryote life with episodic deposits formation in the early-middle Mesoproterozoic period.

2. Geological background and sample description

The Chinese Tianshan belt is located in the southern CAOB that is bounded by the Siberian and European (Baltica) cratons to the north and the Tarim, North China and South China cratons to the south (Fig. 1a and 1b). The belt is divided into the eastern and western Tianshan by the Urumqi-Korla road (Fig. 1b). The eastern Tianshan is tectonically composed of Paleozoic Dananhu arc, Kanggur arc, Yamansu arc and the Precambrian Central Tianshan Block (CTB), separated by Kanggur, Kushui, Aqikuduke and Kawabulak faults (Fig. 1c; Xiao et al., 2004; Charvet et al., 2007; Gao et al., 2009). The CTB is a Precambrian continental fragment with affinity to Fennoscandia (Huang et al., 2019). The crustal basement of the CTB is dominated by Mesoproterozoic granitoids including monzogranites, tonalities and granodiorites with minor diorites and amphibolites (Hu et al., 2006; Shi et al., 2010; He et al., 2015a, 2018). They are covered with Neoproterozoic Xingxingxia and Kawabulak groups (He et al., 2015a, 2018; Huang et al., 2017, 2019). The two groups are composed of *meta*-sedimentary rocks including *meta*-sandstone, marble, schist and quartzite (Li et al., 2002a; Huang et al., 2014, 2015, 2017, 2019). Widespread Neoproterozoic granitoids (1.0–0.7 Ga) are exposed in the CTB and overlain by Cambrian to Permian sedimentary rocks (Xiao et al., 2004; Huang et al., 2017). In this study, samples are collected from the basement of the CTB near Alatagh (Fig. 1c). They are granitoids and were intruded by Paleozoic granites (Fig. 2a). They show foliated and slightly deformed characteristics with gneissic and augen structures (Fig. 2b–2e). These granitoids can be classified as granites in Fig. 3a where two groups of samples are distinguished: samples with lower and higher SiO_2. The granitoids with lower SiO_2 occurred as batholiths and intruded by a late mafic dyke (Fig. 2b). They are medium- to coarse-grained and comprised of quartz (~30 vol%), plagioclase (~30 vol%), K-feldspar (~35 vol%) and biotite (~5 vol%) (Fig. 2d). The granitoids with higher SiO_2 are fine- to medium and have a transitional contact relationship with the lower SiO_2 granitoids in the field (Fig. 2c and 2e). They are characterized by a higher volume of quartz, higher SiO_2 contents but lower proportions of biotites than samples with lower SiO_2. In contrast, the granitoids with higher SiO_2 have a relatively wider range of mineral compositions consisting of quartz (~32–35 vol%), plagioclase (~25–40 vol%), K-feldspar (~10–35 vol%) and biotite (~0–3 vol%) (Fig. 2e).

3. Analytical methods

3.1. Whole-rock geochemistry

Whole-rock major elements were measured on fused glass disks using a Rigaku RIX 2000 X-ray fluorescence spectrometer in the State Key Laboratory of Isotope Geochemistry (SKLIG), Guangzhou Institute of Geochemistry, Chinese Academy of Sciences (GIG–CAS). The analytical precision is within 1–5%. Detailed analytical procedures are described in Li et al. (2006) and the measured reference is consistent with the reported value (http://georem.mpch-mainz.gwdg.de/sample_query.asp), which is listed in Supplementary Table 1. Trace element analyses were conducted by using a Perkin-Elmer Sciex ELAN 6000 ICP–MS in the SKLIG. The analytical procedures are referred to Li et al. (2002b), Li et al. (2007a). The trace elements analytical precision is generally better than 5% (Supplementary Table 1). The measured reference is identical to the recommended value listed in Supplementary Table 1. The whole-rock geochemical data are presented in Supplementary Table 1.

3.2. Zircon U–Pb dating, Lu-Hf-in-zircon and whole rock Nd isotopic analysis

Zircons were collected from each sample using conventional heavy liquids and magnetic separation techniques. Zircons were then hand-picked and mounted in epoxy resin and polished to their half thickness. Cathodoluminescence (CL) imaging was taken for these zircons to reveal their internal structure using a JEOL JXA-8100 Electron Probe with a Mono CL3 Cathodoluminescence System in the SKLIG.

3.2.1. Zircon U–Pb dating

Zircon U–Pb isotope compositions of samples were analyzed using an Agilent 7500a ICPMS equipped with a RESOlution M−50 laser ablation system at the Key Laboratory of Mineralogy and Metallogeny, Guangzhou Institute of Geochemistry, Chinese Academy of Sciences. Energy of the laser ablation was set to 80 mJ, and repletion rate of 8 Hz and a beam size of 31 μm were applied in analysis. Helium was used to transport the ablated sample materials to the ICPMS. Zircon 91500 and silicate glass NIST 610 were used as the standard for zircon U–Pb and trace elements calculations, respectively. During the analyses, the standard 91500 yielded weighted mean $^{206}Pb/^{238}U$ age of 1062 ± 5 Ma (MSWD = 0.15, n = 18), which is consistent with the recommended value (1061 ± 4 Ma, Jackson et al., 2004). Zircon U–Pb isotope ratios were calculated using the ICPMSDataCal program (Liu et al., 2008). The age calculation and plotting were made using Isoplot (ver. 3.00) (Ludwig, 2003). The analytical results are presented in Supplementary Table 2. In this study, uncertainties on individual analysis are reported at 1σ level. Zircon analyses with discordance <95% are not considered for the mean age calculation.

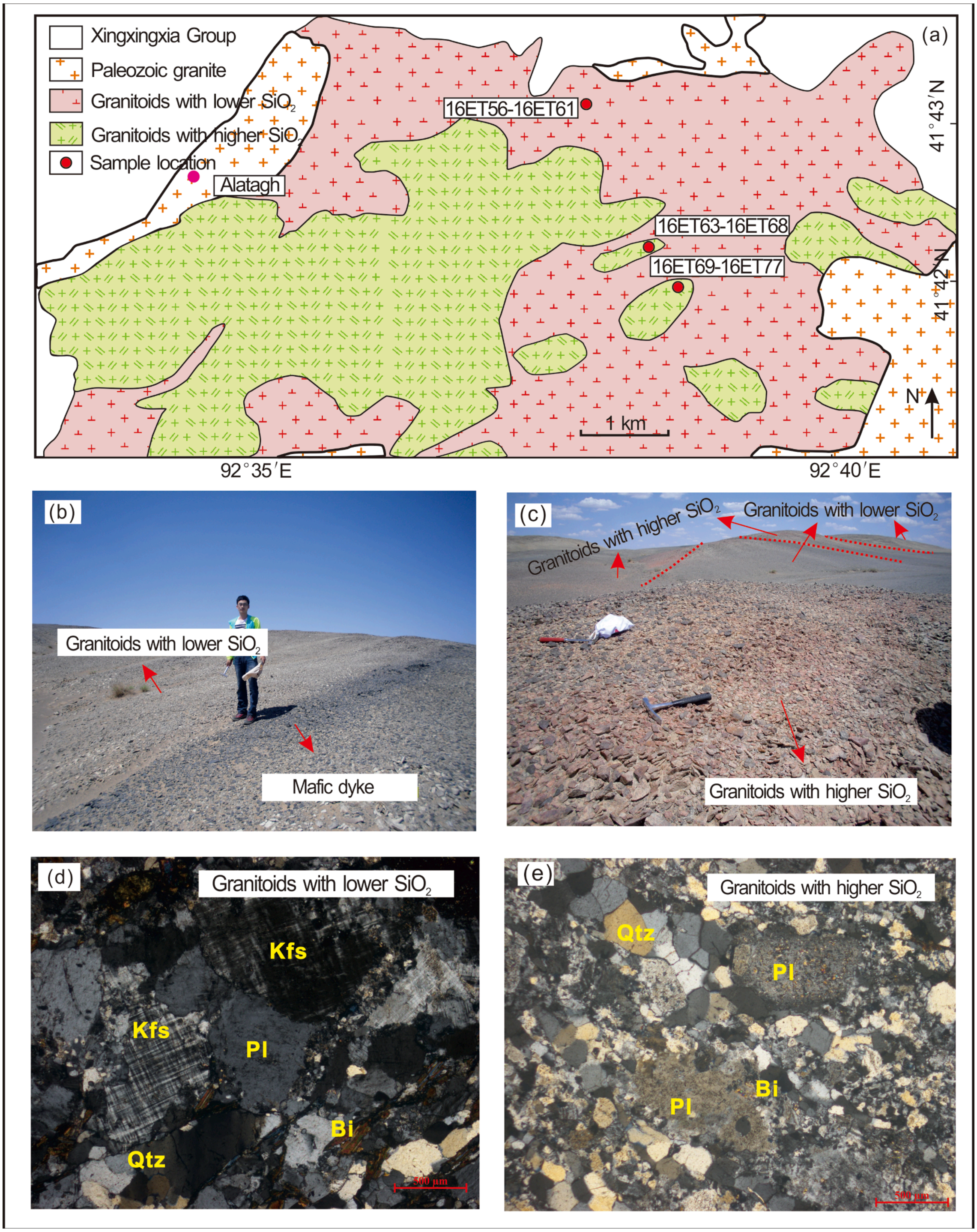

Fig. 2. (a) Geological map of the Alatage in the Chinese Central Tianshan Block showing the sampling sites (after He et al., 2015a). (b-e) Field photographs and Photomicrographs of Mesoproterozoic granitoids. Qtz = quartz; Pl = plagioclase; Kfs = K-feldspar; Bi = biotite.

3.2.2. Lu–Hf–in–zircon isotopic analysis

Hf–in–zircon isotopic analyses were performed on a Neptune Plus MC–ICP–MS (Thermo Scientific), coupled with a RESOlution M−50 193 nm laser ablation system (Resonetics) in the SKLIG, GIG-CAS. The laser parameters of 45 μm diameter beam, 6 Hz repetition rate and ~ 4 $J \cdot cm^{-2}$ energy density were performed on zircon grains for acquiring Hf isotopes. During the analyses, the Helium was the carrier gas, and its blank (^{180}Hf) was < 0.2 mv. The isobaric interferences of ^{176}Lu and ^{176}Yb on ^{176}Hf are corrected by the ratios of $^{176}Lu/^{175}Lu = 0.02656$ and $^{176}Yb/^{173}Yb = 0.79381$ (Segal et al., 2003; Wu et al., 2006). The mass bias factor of Yb is calculated from the measured $^{173}Yb/^{171}Yb$ and the natural ratio of 1.13268. The mass bias factor of Lu is the same as that of Yb. The mass bias of $^{176}Hf/^{177}Hf$ was normalized to $^{179}Hf/^{177}Hf = 0.7325$ with an exponential law. The detailed data reduction procedure is reported in Zhang et al. (2015a) and Zhang et al. (2015b). Standard zircons Penglai was used as the external standard and was analyzed twice before and after every 5 analyses of unknowns. Repeated 22 Penglai measurements yielded a weighted mean of $^{176}Hf/^{177}Hf$ at 0.282476 ± 8 (SD), which is consistent with the reported value within errors (0.282482 ± 0.000013, Sláma et al., 2008). The measured

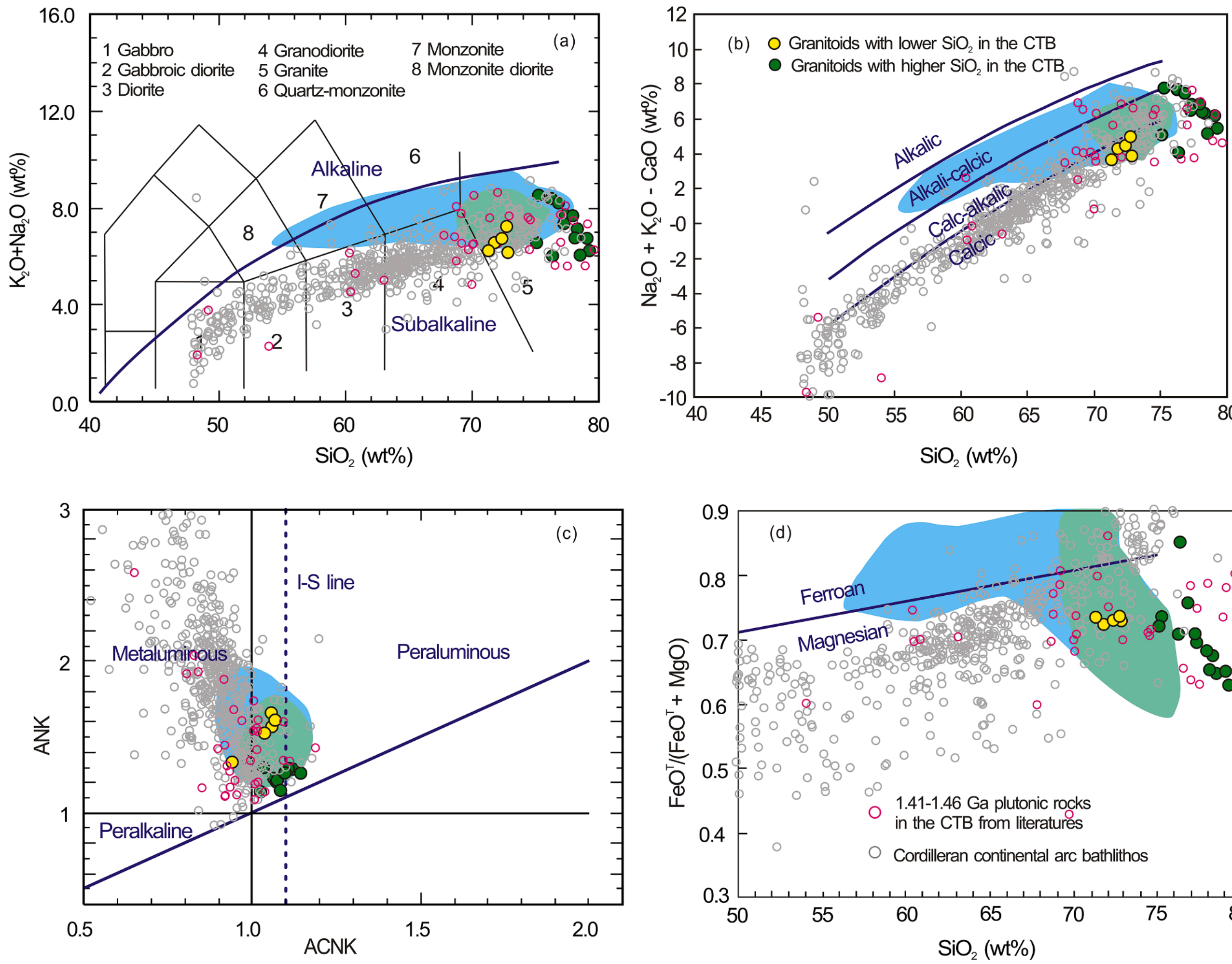

Fig. 3. Classification diagrams for the studied Mesoproterozoic granitoids to compare with melts from medium- to high K basaltic rocks and the arc plutons from Cordillera. (a) Total alkali-silica (TAS) classification diagram (Middlemost, 1994); (b) Na_2O + K_2O - CaO versus SiO_2, (c) ANK versus ACNK diagram (Maniar and Piccoli, 1989); (d) $FeO^T/(FeO^T + MgO)$ versus SiO_2 diagram (Frost et al., 2001). Data for 1.41–1.46 Ga plutonic rocks in the CTB is summarized in Supplementary Table 5. Data for Cordilleran continental arc batholiths is also summarized in Supplementary Table 5, which is from Lee et al. (2007); http://georoc.mpch-mainz.gwdg.de/georoc/ and https://www.navdat.org/. Experimental melts in blue color for medium- to high K basaltic rocks at 7 kbar, 825–925 °C are from Sisson et al. (2005). Melts formed at melting temperature lower than 850 °C with SiO_2 > 70 wt% from medium- to high K basaltic rocks are highlighted in green.

$^{176}Lu/^{177}Hf$ ratios and the ^{176}Lu decay constant of 1.867 × 10^{-11} a^{-1} (Söderlund et al., 2004) were used to calculate initial $^{176}Hf/^{177}Hf$ ratios. The ε_{Hf} (t) values are calculated from chondritic values of $^{176}Hf/^{177}Hf$ = 0.282785 and $^{176}Lu/^{177}Hf$ = 0.0336 (Bouvier et al., 2008). The depleted mantle line is defined by present-day $^{176}Hf/^{177}Hf$ = 0.28325 and $^{176}Lu/^{177}Hf$ = 0.0384 (Griffin et al., 2004). $^{176}Lu/^{177}Hf$ ratio of 0.015 for the average continental crust (Griffin et al., 2002) was used to calculate two-stage (crustal) model ages (T_{DM}^{C}). The Lu–Hf isotopic data are listed in Supplementary Table 3.

3.2.3. Whole rock Nd isotopic analysis

Nd isotopic analyses were carried out at SKLIG, GIG-CAS. The Nd isotopic measurements are performed using a Neptune Plus multi-collector mass spectrometry (MC-ICP-MS). Analytical procedures can be found in Wei et al. (2002) and Li et al. (2004). Normalizing factor used to correct the mass fractionation of Nd during the measurements is $^{146}Nd/^{144}Nd$ = 0.7219. Analyses of standards Shin Etsu JNDi-1 over the measurements period provided $^{143}Nd/^{144}Nd$ ratio of 0.512119 ± 5 (SD, n = 3), which is identical to the recommended value ($^{143}Nd/^{144}Nd$ = 0.512115 ± 7, Tanaka et al., 2000). The BHVO-2 reference materials were run as unknowns and yielded $^{143}Nd/^{144}Nd$ = 0.512973 ± 4, which is consistent with the recommended value ($^{143}Nd/^{144}Nd$ = 0.512983 ± 10, Weis et al., 2005). The Nd isotopic results are listed in Supplementary Table 4.

4. Results

4.1. Whole-rock major and trace element geochemistry

The studied samples have high SiO_2 (71.32–79.26 wt%) and are plotted in a granite field with a variety of K_2O contents (Fig. 3a and Supplementary Table 1). These studied samples are also calcic to calc-alkaline (Fig. 3b). These samples show metaluminous to slightly peraluminous characteristics with aluminum saturation index (ASI) (A/CNK = $Al_2O_3/(CaO + Na_2O + K_2O$, molecular ratio) varying between 0.94 and 1.14 (Fig. 3c). Their relatively low FeO^T (0.42–2.87 wt%) contents make them magnesian characteristics (Fig. 3d). These samples also have low Zr (52.9–162 ppm), Nb (0.84–8.35 ppm), Ce (16.8–70.5 ppm), Y contents (2.33–18.4 ppm) and low 10000 Ga/Al ratios (1.16–2.25) (Supplementary Table 1) relative to A-type granites (Fig. 4a-4c). Moreover, these samples show relatively low zircon saturation temperatures between 642 °C and 745 °C, which are comparable to those of Cordilleran continental arc batholiths but significantly lower than those of plume-related granitic rocks (Fig. 4d). Overall, these

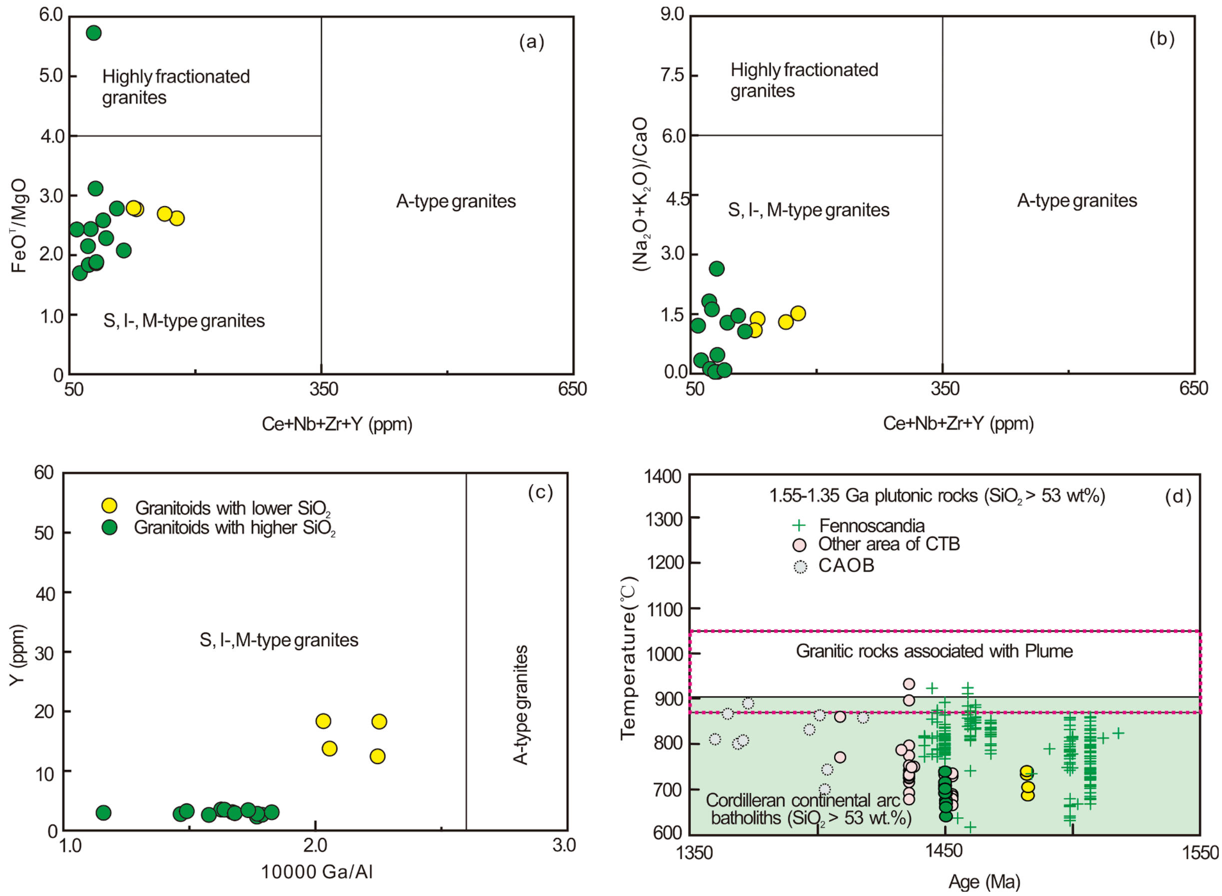

Fig. 4. (a–c) Diagrams defining highly fractionated granites and A-type granites (Whalen et al., 1987) and (d) zircon saturation temperature (T_{Zr}) (Boehnke et al., 2013). (a) FeO^T/MgO versus Ce + Nb + Zr + Y, (b) $(Na_2O + K_2O)/CaO$ versus 10000 Ga/Al, (c) Y versus Ce + Nb + Zr + Y for the Mesoproterozoic granitoids in the Chinese Central Tianshan Block. (d) Zircon saturation temperature for the plutonic rocks from this study, other area of the CTB (Hu et al., 2006; Shi et al., 2010; He et al., 2015a), CAOB (Kröner et al., 2013; Han et al., 2017; Yuan et al., 2019) and Fennoscandia (Andersson, 1997; Čečys et al., 2002; Obst et al., 2004; Motuza et al., 2006; Skridlaitė et al., 2007; Roberts et al., 2013; Johansson et al., 2016). The red dash box is the zircon saturation temperatures of granitic rocks associated with plume (Campbell, 2001; Xu et al., 2001; Ernst and Buchan, 2003; Liu et al., 2014a). The green area is the zircon saturation temperature of Cordilleran continental arc batholiths with SiO_2 > 53 wt% (Supplementary Table 5).

samples display continental arc-like light rare earth element (LREE) enrichments ($(La/Yb)_N = 12.4–51.3$) with depletion of Nb, Ta and Ti and display positive to negative Eu anomalies ($Eu/Eu^* = 0.62–2.69$) (Fig. 5a and 5b).

Noticeably, a decreasing trend of P_2O_5 with increasing SiO_2 was observed. The granitoids with higher SiO_2 have lower P_2O_5 as well as TiO_2, MgO, FeO^T, Nb, Nb/Ta and Dy/Yb together with low Ba and Sr than those with lower SiO_2 (Fig. 6a–6h). The former are characterized by middle REE fractionation, while the latter have unfractionated heavy REE patterns (Fig. 5a).

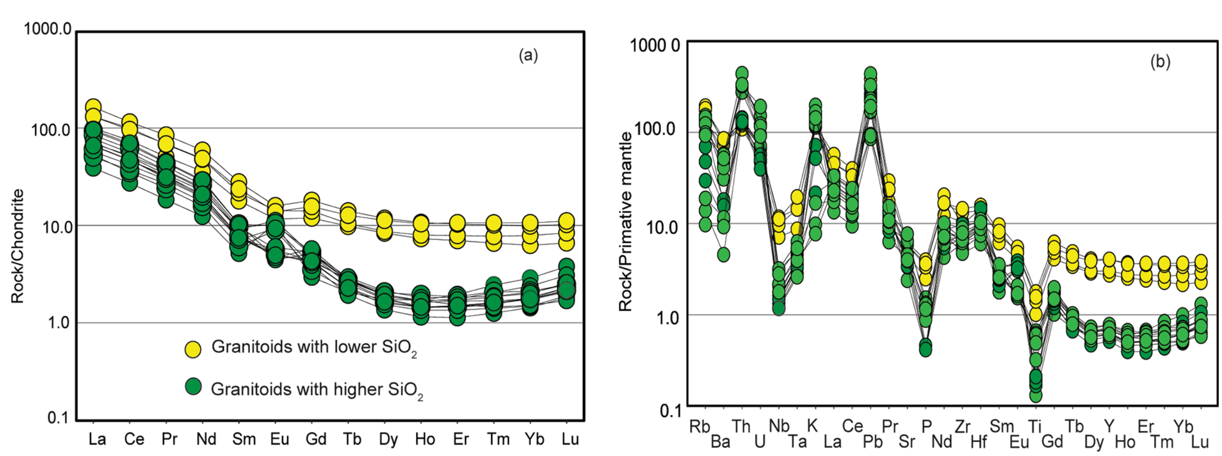

Fig. 5. Chondrite-normalized REE patterns and primitive mantle-normalized trace element variation diagrams for studied Mesoproterozoic granitoids. Normalizing values are from Sun and McDonough (1989).

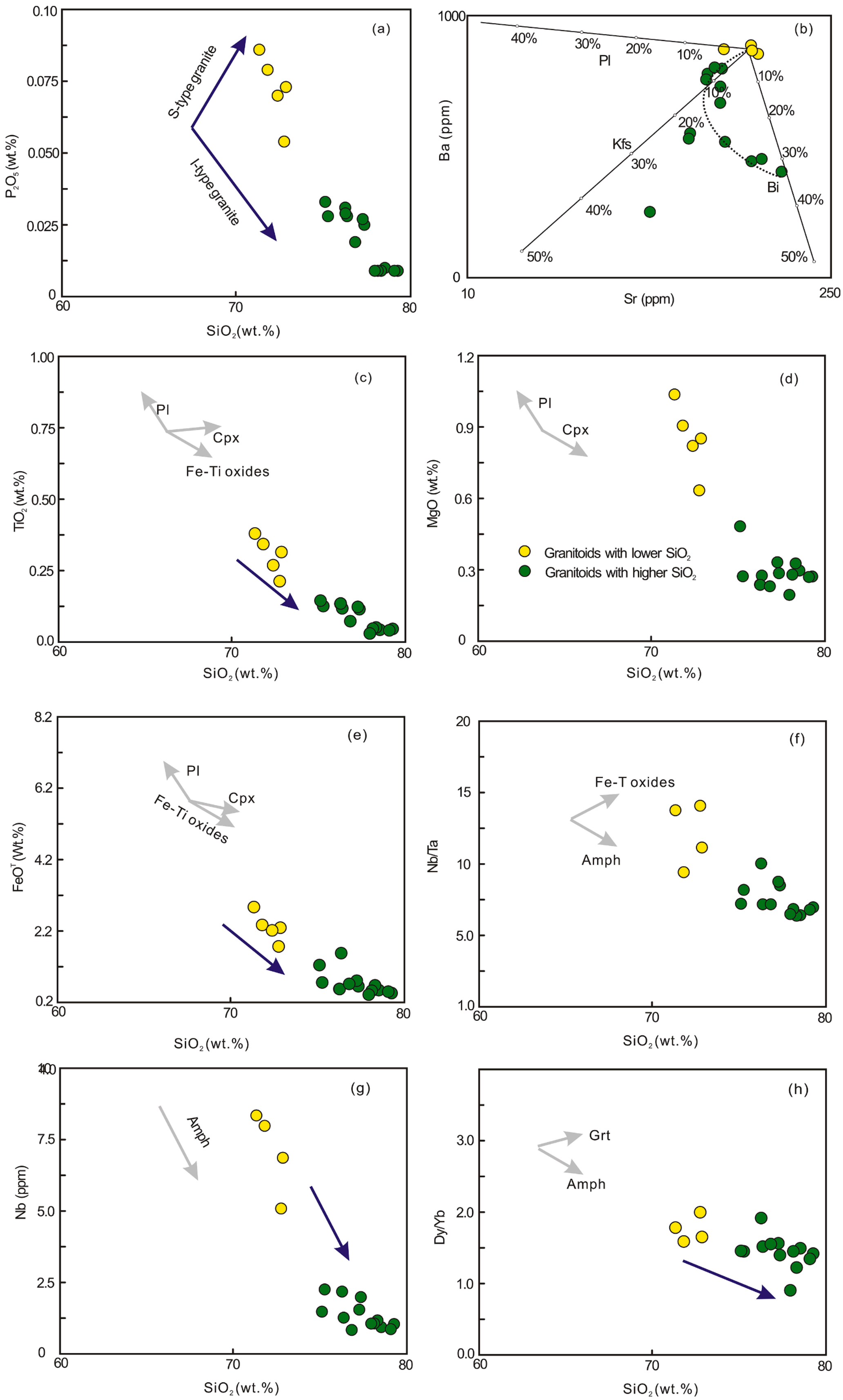

Fig. 6. (a) Diagram of P_2O_5 versus SiO_2 to distinguish the I-type and S-type granites. (b) Ba versus Sr diagram showing that fractionation of K-feldspar and biotite plays an important role in formation of granitoids with higher SO_2. Partition coefficients of Ba and Sr are from Hanson (1978). (c–h) Bivariate plots of elements versus SiO_2 to address origin of the Mesoproterozoic granitoids in the Central Tianshan Block. Amph = amphibole; Bi = biotite; Cpx = clinopyroxene; Fe-Ti oxides = Fe-Ti bearing oxides (titanite ilmenite, or rutile); Grt = garnet; Pl = plagioclase; Kfs = K-feldspar.

4.2. U-Pb geochronology, Hf-in-zircon and whole-rock Nd isotopic composition

Zircon grains of granitoids with lower SiO_2 (16ET56) in the CTB have been dated. They are transparent and euhedral, and most have prismatic shapes with well-developed oscillatory zoning, suggesting an igneous origin (Hoskin and Schaltegger, 2003, Fig. 7a). Among twenty five analyzed spots, two are of metamorphic rims (1433 Ma and 1436 Ma) and three show high U (>2000 ppm) contents (Supplementary Table 2, Fig. 7a). Ten spots show discordant results due to lead loss, with $^{206}Pb/^{238}U$ ages between 1307 Ma and 1583 Ma (Supplementary Table 2, Fig. 7a). The above metamorphic and high U zircons as well as discordant analyses were not considered in the mean age calculation. The emplacement age is thus calculated based on the ten concordant results with $^{206}Pb/^{238}U$ ages varying from 1480 to 1484 Ma, which yields a weighted mean $^{206}Pb/^{238}U$ age at 1482 Ma ± 8 Ma (Fig. 7b).

Hf-in-zircon isotopic compositions are calculated using the mean age of 1482 Ma for ten concordant analyses, two spots of metamorphic rims and three analyses of high U zircons. These measured $^{176}Hf/^{177}Hf$ ratios are similar (Supplementary Table 3), suggesting that metamorphim or high U contents effects did not affect Hf isotope composition. Thus these fifteen analyses yield similar high initial $^{176}Hf/^{177}Hf$ ratios (0.281951 to 0.282056), equivalent to positive ε_{Hf} (t) values (+3.9 to + 7.6) (Supplementary Table 3). These zircons also display relatively young crustal model ages (T^C_{DM} = 1.7 – 2.0 Ga) (Supplementary Table 3). Meanwhile, the granitoids with lower SiO_2 (18ET56) have positive whole-rock ε_{Nd}(t) values (+1.14 to + 1.22), except one showing a slightly negative value of −0.54 (Supplementary Table 4). They have relatively young Nd model ages (T^2_{DM} = 1.9–2.1 Ga) similar to T^C_{DM} (Supplementary Table 4).

Sample 16ET69 of the granitoids with higher SiO_2 in the CTB was selected for dating. Zircon grains from the 16ET69 are mostly euhedral and prismatic with lengths ranging from 100 to 250 μm and length/width ratios of 1:1 to 2.5:1. Most grains are transparent and display oscillatory zoning, suggesting an igneous origin (Hoskin and Schaltegger, 2003, Fig. 7c). Some are dark in color exhibiting blurred and complicated textures (Fig. 7c). Among thirty-three zircons analyzed, twenty-one transparent grains yielded concordant results with $^{206}Pb/^{238}U$ ages between 1445 and 1456 Ma (Fig. 7c, Supplementary Table 2). Five are high-U grains (>2000 ppm, Supplementary Table 2) with three being discordant in age and six spots also deviate from the concordant line (Fig. 7c). The high U and discordant zircons, together with an inherited grain, were not considered in the mean age calculation. The emplacement age of 16ET69 thus can be calculated with a weighted mean $^{206}Pb/^{238}U$ age of 1450 ± 7 Ma (Fig. 7d). This age is consistent with the formation age of granitoids with lower SiO_2 whin errors and matches with those in other parts of CTB (Fig. 1b and Supplementary Table 5). Zircons from the granitoids with higher SiO_2 possess similarly positive ε_{Hf} (t) values (+2.3 to + 7.8) with correspondingly young crustal model ages (T^C_{DM} = 1.7 – 2.1 Ga) (Supplementary Table 3). Additionally, granitoids with higher SiO_2 have positive whole-rock ε_{Nd} (t) values (+0.22 to + 0.99) with T^2_{DM} model ages of 1.9–2.0 Ga, which couple with the Hf isotopic compositions (Supplementary Tables 4).

5. Discussion

5.1. Petrogenesis of the Mesoproterozoic granitoids in the CTB

Before discussing the petrogenesis for the Mesoproterozoic granitoids, effects of post-magmatic processes on elemental mobility are

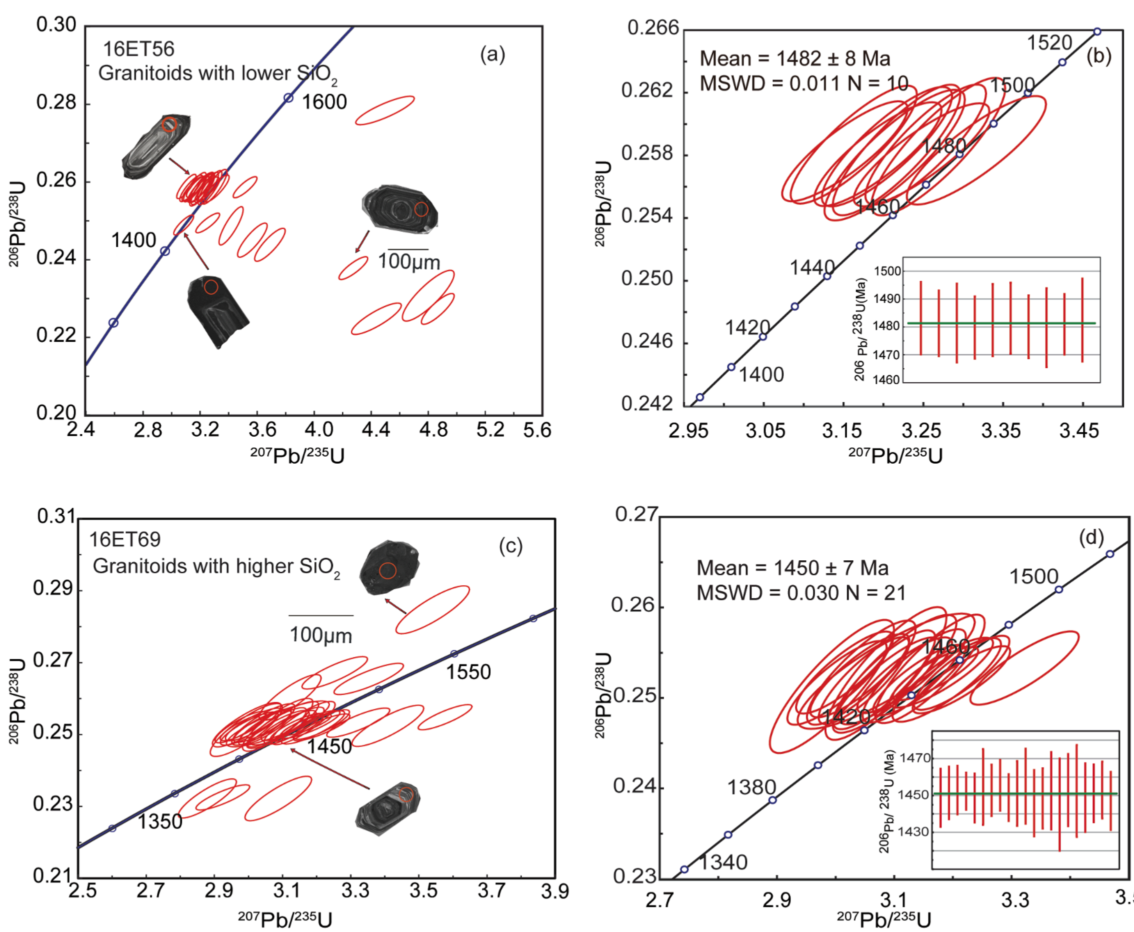

Fig. 7. LA–ICPMS zircon U–Pb concordia diagrams for the studied Mesoproterozoic granitoids.

needed to be assessed (e.g., alteration, deformation and metamorphism). The granitoids have relatively low loss on ignition values (LOI) values (<1.5 wt%), suggesting little influence by post-magmatic processes. The effects can also be evaluated by the relationship between elements and chemical index of weathering [CIW = Al_2O_3/(Al_2O_3 + CaO + Na_2O), molecular ratio; Harnois, 1988]. For example, the good correlations between CIW and elements indicate that these elements are potentially distributed by alteration and deformation or metamorphism processes (Wang et al., 2010a). Major oxides (e.g. Na_2O, K_2O, CaO, Al_2O_3, P_2O_5, $Fe_2O_3^T$ and MgO) and trace elements (Rb, Sr and Ba) show no correlation with CIW in the studied samples (Supplementary Figure S1), indicating insignificant mobilization during the post-magmatic processes. High field strength elements (e.g., Nb, Ta, Zr, Ti) have been suggested to remain immobile to these processes (Polat et al., 2002; Ordóñez-Calderón et al., 2008). Consistency in rare earth elements and in Nd-Hf isotopic compositions also precludes effects from post-magmatic processes on the elemental mobility. Accordingly, the elements can be used to decipher the petrogenesis.

These Mesoproterozoic granitoids have high SiO_2 contents (71.32–79.26 wt%) similar to highly fractionated granites (Wu et al., 2003; Perez-Soba and Villaseca, 2010). However, the granitoids are deficient of aluminum-rich minerals (e.g., lithium mica, tourmaline beryl, Fig. 2d and 2e) that commonly present in highly fractionated granites (Chudík et al., 2008; Černý et al., 2012; Merino et al., 2013; Li et al., 2015; Wu et al., 2017). Low FeO^T/MgO and (Na_2O + K_2O)/CaO ratios also preclude a highly fractionated granites origin (Fig. 4a and 4b). Extensive fractionation of plagioclase is an important process to generate highly fractionated granites, which would show strong Eu depletion (Miller and Mittlefehldt, 1982; Wu et al., 2003, 2017; Gelman et al., 2014). Nevertheless, the Mesoproterozoic granitoids have limited fractionation of plagioclase with weakly negative to strongly positive Eu anomalies (Fig. 5a). This disparity does not support a highly fractionated granites affinity. Most highly fractionated granites also possess characteristics of REE tetrad effect because of separation of accessory minerals (e.g., apatite, zircon, allanite and monazite) (Wu et al., 2003, 2017). The dearth of tetrad effect of the Mesoproterozoic granitoids also precludes a highly fractionated granites origin (Fig. 5a). Therefore, the Mesoproterozoic granitoids in this study are not highly fractionated.

Granites can be subdivided into M, A, S, and I types according to their source characteristics (Whalen et al., 1987; Chappell and White, 1992). M-type granites are considered to have low K_2O contents (<2.0 wt%), but high MgO contents (>2.0 wt%) (Whalen, 1985; Maurice et al., 2013). The Mesoproterozoic granitoids have higher K_2O (average 3.3 wt %) and lower MgO contents (0.20–0.91 wt%) (Supplementary Table 1), suggesting an unlikely affinity to M-type granites. A-type granites typically have iron-rich and alkali mafic minerals (e.g., Fe-rich biotite/amphibole, sodic amphibole/pyroxene and aegirine-augite) and limited plagioclase (Chappell and White, 1992; Wu et al., 2002; Bonin, 2007; Wang et al., 2010b). A-type granites are also characterized by ferroan compositions and have higher Zr + Nb + Ce + Y contents, Ga/Al ratios as well as higher zircon saturation temperatures (830–1000 °C) compare to S- and I-type granites (Clemens et al., 1986; Whalen et al., 1987; Chappell and White, 1992; Eby, 1992; Frost et al., 2001; Frost and Frost, 2011). Mafic minerals are absent in the Mesoproterozoic granitoids (Fig. 2e and 2e), which is distinct from the A-type granite. Moreover, the magnesian characteristics, low Ce + Nb + Zr + Y contents and Ga/Al ratios together with low zircon saturation temperatures (642–745 °C, Fig. 3d and 4a–4d) of the Mesoproterozoic granitoids argue against an A-type granite origin. Basically, S-type granites are composed of Al-rich minerals (muscovite, cordierite and garnet), and are marked by strongly peralumious compositions with Alumina Saturation Index (ACNK) higher than 1.1 (Chappell and White, 1992). The paucity of Al-rich mineral and metaluminous to slightly peraluminous compositions (ACNK = 0.94 ~ 1.1) of the studied Mesoproterozoic granitoids clearly distinguish them from S-type granites. The relationship between P_2O_5 and SiO_2 is effective in distinguishing S- and I-type granites, which are characterized by positive and negative relationships, respectively (Chappell and White, 1992; Chappell, 1999; Li et al., 2007b; Clemens et al., 2011). The Mesoproterozoic granitoids display a decreasing P_2O_5 with increasing SiO_2 (Fig. 6a), indicative of nature of I-type granites.

5.2. Origin of the Mesoproterozoic granitoids in the CTB

Generation of I-type granites can be achieved from two broad mechanisms: extensive fractional crystallization of mantle-derived magma or partial melting of crustal igneous rocks (Chappell and White, 1974; Chappell and Stephens, 1988; Chappell, 1999; Frost et al., 2016; Ulmer et al., 2018; Gao et al., 2020). Extensive fractional crystallization occurring in mantle-derived magma could give rise to abundance of mafic–ultramafic cumulates (Clemens and Stevens, 2012). Nevertheless, rare mafic–ultramafic rocks associated with the Mesoproterozoic granitoids are observed in the CTB. Furthermore, petrological experiment studies have suggested that fractional crystallization of mantle-derived melts could produce metaluminious to weakly peraluminous compositions with SiO_2 contents of 56–60 wt% (Ulmer et al., 2018). The Mesoproterozoic granitoids are metaluminious to weakly peraluminous with SiO_2 contents of 71.32–79.26 wt%, which suggests that they were not directly derived from extensive fractional crystallization of a mantle-derived magma. The Mesoproterozoic granitoids have positive Hf–Nd isotopic compositions (Supplementary Tables 3 and 4), suggesting that they have mafic crust related source. The granitoids with lower SiO_2 have medium- to high K_2O components (Supplementary Table 1), which preclude a low K mafic source. Petrological experiment studies have showed that melts from partial melting of medium- to high K basaltic rocks at 7 kbar have a relatively high SiO_2 of 57.10–75.60 wt % and high K_2O of 2.29–5.39 wt% (Sisson et al., 2005), which are in agreement with those of the Mesoproterozoic granitoids (Fig. 3a, SiO_2: 71.32–72.85 wt%, K_2O: 3.45–4.13 wt%, this study). It is true especially for those melts formed at melting temperature lower than 850 °C with SiO_2 > 70 wt%, as they share similar subalkaline, calcic, metaluminious to weakly peralumious compositions and magnesian characteristics with the Mesoproterozic granitoids (Fig. 3a–3d, green area). It is thus suggested that partial melting of medium-to high K basaltic rocks formed the granitoids with lower SiO_2 in this study at temperature lower than 850 °C. This matches with the low zircon saturation temperatures (694–745 °C) calculated for the Mesoproterozoic granitoids (Fig. 4d).

Linear trends on major and trace elements between the granitoids suggest that they are genetically related with fractional crystallization (Fig. 6b-6h). In the diagram of Ba vs Sr (Fig. 6b), Sr and Ba contents of the granitoids decrease slowly at the beginning, followed by a drastic drop. These features suggest that a probable early limited fractionation of plagioclase, followed by crystallization of K-feldspar and biotite from the granitoids with lower SiO_2 to form those with higher SiO_2. The decrease in TiO_2 with increasing SiO_2 precludes a clinopyroxene fractionation in the Mesoproterozoic granitoids (Fig. 6c). This is because fractional crystallization of clinopyroxene can cause a decrease of MgO and FeO^T contents but lead to an increase of TiO_2 contents (Fig. 6c to 6e, Nagasawa and Schnetzler, 1971; Ewart et al., 1973; Stimac and Hickmott, 1994; Huang et al., 2006). Crystallization of Ti-bearing oxides (titanite, ilmenite, or rutile) could lower TiO_2 and FeO^T with increasing SiO_2 contents, whereas this process could also result in an increasing tendency of Nb/Ta ratios (Stepanov et al., 2014). A decreasing trend of Nb/Ta ratios with increasing SiO_2 can be observed in the Mesoproterozoic granitoids and argue against a Fe-Ti oxides fractionation (Fig. 6f). Fractionation of amphibole instead could give rise to a decrease in Nb content and correspondingly a decrease in Nb/Ta (Stepanov et al., 2014). These features are consistent with the decreasing trend of Nb/Ta and Nb contents in the Mesoproterozoic granitoids (Fig. 6f and 6g). The decreasing Dy/Yb with increasing SiO_2 and the depletion of the middle REEs also support the fractionation of amphibole rather than garnet (Fig. 5a and 6h). Amphibole preferentially incorporates middle REES, whereas garnet incorporates heavy REEs over the middle REEs

(Davidson et al., 2007). Consequently, separation of amphibole will cause decrease in Dy/Yb ratios and depletion in middle REEs, but crystallization of garnet will increase the Dy/Yb ratios and cause strong depletion in heavy REEs relative to middle REE (Pertermann et al., 2004; Macpherson et al., 2006; Davidson et al., 2007). Therefore, these trends and REEs patterns indicate amphibole rather than garnet crystallization for the Mesoproterozoic granitoids. These characteristics might be affected by accessory minerals (such as apatite, allanite and monazite), since these minerals have partition coefficients (Kd) >1 for REEs (e.g., $Kd_{Nd} > Kd_{Yb}$, Wu et al., 2003 and reference therein). Consequently, separation of these accessory minerals could lead to a decrease in Nd/Yb ratio. However, compared to the granitoids with lower SiO_2 in this study, those with higher SiO_2 have higher Nd/Yb ratios (Supplementary Table 1), precluding the influence from the accessory mineral separation. The increase of the Nd/Yb ratios further confirm the major role of the amphiboles in causing the Dy/Yb decrease and depletion of the middle REEs in the granitoids, as amphiboles usually prefer HREE than LREE ($Kd_{Nd} < Kd_{Yb}$) in a system (Davidson et al., 2007). These differences thus indicate that the granitoids were formed in an amphibole stable field without garnet occurrence, which could happen in a depth of no more than 30 km (Pertermann et al., 2004; Davidson et al., 2007; Palin et al., 2016; Li et al., 2017). Combined with the low calculated zircon saturation temperatures (642–745 °C), the above evidence thus reflects that the granitoids with lower SiO_2 differentiated to form those with higher SiO_2 by factional crystallization, they were both formed in an amphibole-stable field at temperature lower than 850 °C.

5.3. Tectonic setting for the Mesoproterozoic granitoids in the CTB

The studied Mesoproterozoic granitoids are magnesian, calcic to calc-alkalic and metaluminous to slightly peraluminous (ACNK = 0.94–1.1) (Fig. 3b and 3c), which are comparable to arc-like granites. They possess typical arc-like trace element distribution patterns with significant enrichment in large ion lithophile elements (e.g., Rb, Th, Pb) but depletion in high field strength elements (e.g., Nb, Ta, Ti, Fig. 5a and 5b). The granitoids associated with monzogranites, tonalities, granodiorites and minor diorites and amphibolites make up the Mesoproterozoic crustal components of CTB (Hu et al., 2006; Shi et al., 2010; He et al., 2015a, 2018). These crustal components are analogous to the batholiths of Mesozoic Cordillera which is the representative of active continental margin arc comprised mainly of monzogranites, tonalities and granodiorites, as well as subordinate diorites and gabbros (Fig. 3a, Lee et al., 2007; Ducea et al., 2015; Collins et al., 2020). Crustal components in CTB and batholiths of Mesozoic Cordilleran continental arc have consistent compositions (Fig. 3a, 3b and 3c). Moreover, the granitoids in the CTB share indistinguishable low zircon saturation temperatures (642–745 °C) and are plotted in an arc granite field as those of Mesozoic batholiths in the Cordilleran continental arc (Fig. 4d, 8a and 8b, Supplementary Table 1 and Table 5). In this regard, it manifests that the CTB was an active continental margin in Mesoproterozoic, analogues to the Mesozoic Cordilleran continental arc. This correspondingly indicates a subduction affinity for the studied granitoids. An 1.46–1.38 Ga magmatic belt extends 100–240 km along the margin of CTB (Fig. 1b, Hu et al., 2006; Shi et al., 2010; He et al., 2018), which further supports the subduction association.

5.4. The cause for Nuna breakup

The cause for the breakup of Nuna remains unknown due to the lack of oceanic lithosphere and oceanic plume records in the period of Nuna breakup. Recognizing ancient subduction and plume related events is thus essential to illuminate the dynamic mechanism at the time of the breakup of Nuna. Single geochemical or geological evidence can hardly be able to unambiguously discriminate the ancient plume from subduction (Campbell, 2001; Xu et al., 2013). A comprehensive study of both geochemical and geological perspectives is thus required to distinguish the relationship of subduction and plume with the dispersal of Nuna. First, the distinct geochemical characteristics of granitoids related to subduction or plume can help to discern their links to Nuna breakup. Granitoids formed in arcs are subduction-related with a relatively low temperature (e.g., Mesozoic Cordilleran continental arc < 800 °C), and usually developed as a granitic belt (Tatsumi and Eggins, 1995; Stern, 2002; Zheng, 2019). By comparison, granitoids associated with a plume commonly formed under relatively high temperature condition (Campbell, 2001; Ernst and Buchan, 2003; Liu et al., 2014a). Second, trace element proxies like Nb/Yb, Nb/La, Ce/Pb and Nb anomalies in mafic to intermediate rocks can be utilized to discriminate subduction from plume impact on the fragmentation of Nuna. Subduction-related mafic to intermediate rocks tend to have lower ratios of the above element ratios and Nb anomalies with arc signatures than their plume-related counterparts with OIB signatures (Sun and McDonough, 1989; Pearce and Peate, 1995; Campbell, 2001; Kelemen et al., 2003, 2014; Pearce, 2008; Tang et al., 2017; Han et al., 2019; Zheng, 2019). Moreover, metamorphic events can provide clues about the relationship of subduction and plume with the dispersal of Nuna. Generally, a trench-parallel accretionary belt with orogenic metamorphism can probably be observed along a subduction zone (Banno et al., 1978; Tatsumi and Eggins, 1995; Brown, 1998; Ernst, 2005). Trench retreat (e.g., slab rollback) along with crustal thinning and trench advance (e.g., plat subduction) accompanied by crustal thickening commonly occur in a subduction zone (Collins, 2002; Cawood et al., 2009). By contrast, plume tends to cause lithospheric extension and leads to large igneous provinces with radial mafic dykes followed by high-temperature regional metamorphism (White and McKenzie, 1989; Hooper, 1990; Campbell, 2001, 2007; Xu et al., 2001).

5.4.1. A critical cause to drive Nuna breakup

Studies on granitoids in the CTB, CAOB and Fennoscandia indicate that the breakup of Nuna is coeval with a subduction system. The 1.46–1.41 Ga Mesoproterozoic granitoids in the CTB have arc-like characteristics falling into the volcanic arc granite field with relatively low temperatures (Fig. 3d, 8a and 8b), which reflects a subduction-related origin. The 1.45–1.36 Ga granitoids located in the other part of the CAOB likewise display arc signatures comparable to those in the CTB (Fig. 8a and 8b, Supplementary Table 5). These Mesoproterozoic arc-related rocks together compose an arc belt along the margin of CAOB (He et al., 2018; Yuan et al., 2019), which supports the existence of a huge subduction system coeval with Nuna's breakup. The CTB has been suggested to be a part of the Fennoscandia located in the periphery of Nuna (Huang et al., 2019), thus the Mesoproterozoic magmatism in the Fennoscandia could also provide clues regarding the cause for Nuna's breakup. The Mesoproterozoic magmatism in the Fennoscandia exhibits a subduction affinity comparable to that of the CTB counterpart (Fig. 8a and 8b, Supplementary Table 5). The 1.66–1.38 Ga felsic rocks are characterized by tholeiitic to calc-alkalic compositions in the Fennoscandia, and have been suggested to be formed in an arc setting (Andersen et al., 2004; Åhäll and Connelly, 2008; Brander and Söderlund, 2009; Roberts et al., 2013; Roberts and Slagstad, 2015; Ulmius et al., 2015; Bingen and Viola, 2018). These arc-related rocks are aligned along E–W trending, which reveals the pre-existence of an exterior ocean surrounding Fennoscandia (Skridlaitė et al., 2007; Roberts et al., 2013; Huang et al., 2019). Such a close spatial and temporal coincidence of subduction system occurred along the CTB and Fennoscandia discloses a critical role of exterior subduction on the fragmentation of Nuna. The arc-related magmatism was temporally coeval to Nuna's breakup, suggesting that the subduction system may substantially contribute to the Nuna's dispersal. The existence of this subduction system is also supported by the orogeny-related 1.49–1.37 Ga high-grade metamorphism along the periphery of Nuna, as has shown in the CTB and Fennoscandia (Brander and Söderlund, 2009; Ulmius et al., 2015; Zong et al., 2017). Overall, Mesoproterozoic arc magmatism widely existed along the CTB, CAOB and the Fennoscandia, probably

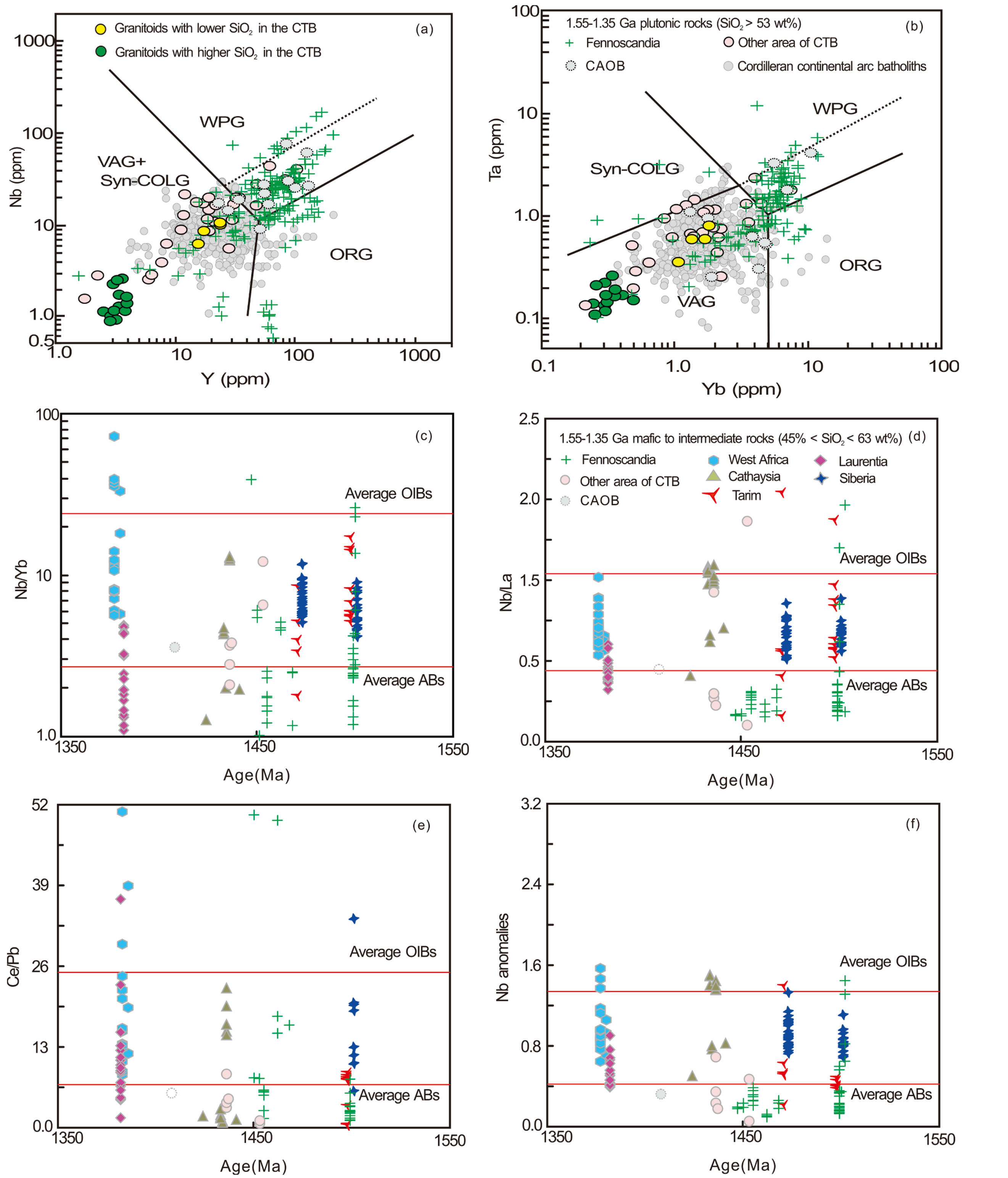

Fig. 8. (a-b) Tectonic discrimination diagram according to Pearce et al. (1984), VAG = volcanic arc granite, Syn-COLG = syncollision granite, WPG = within plate granite, ORG = ocean ridge granite. Data for 1.55–1.35 Ga plutonic rocks from other area of the CTB (Hu et al., 2006; Shi et al., 2010; He et al., 2015a), CAOB (He et al., 2015b; Kröner et al., 2013; Han et al., 2017; Yuan et al., 2019) and Fennoscandia (Andersson, 1997; Claesson and Kresten, 1997; Čečys et al., 2002; Obst et al., 2004; Motuza et al., 2006; Skridlaitė et al., 2007; Roberts et al., 2013; Johansson et al., 2016). (c-f) Plots showing the variations of elemental ratios of mafic to intermediate rocks globally between 1.55 Ga and 1.35 Ga (45 wt% < SiO_2 < 63 wt%). Nb anomaly = $(Nb/0.713)/\sqrt{[(Th/0.085)\times(La/0.687)]}$, normalized by the Primitive Mantle (Sun and McDonough, 1989). Abs = continental and oceanic arc basalts (average value from Kelemen et al., 2003); OIBs = oceanic island basalts (average value from Sun and McDonough, 1989). Date from other area of the CTB (Hu et al., 2006; He et al., 2015a), CAOB (He et al., 2015b) and Fennoscandia (Andersson, 1997; Čečys et al., 2002; Motuza et al., 2006; Skridlaitė et al., 2007; Brander and Söderlund, 2009; Roberts et al., 2013), Laurentia (Upton et al., 2005), West Africa (Bahat et al., 2013), Cathaysia (Zhang et al., 2018c), Tarim (Wu et al., 2014; Wang et al., 2018) and Siberia (Ernst et al., 2016b; Gladkochub et al., 2016). All data are listed in Supplementary Table 5.

reflect a long-lasting subduction system causing the breakup of Nuna.

Among magmatic rocks associated with the breakup of Nuna, a few Mesoproterozoic granitoids in the CAOB and Fennoscandia show affinities to within-plate rocks with relatively high temperatures analogous to those of plume (Fig. 3d, 8a and 8b), and coeval mafic to intermediate rocks from these areas also exhibit involvements of plume materials, as shown by Nb/Yb, Nb/La, Ce/Pb ratios and Nb anomalies (Fig. 8c to 8f). Temporally, these ratios reflect a transition from OIBs to arc signatures in the CTB, CAOB and Fennoscandia (Fig. 8c to 8f, Supplementary Table 5), implying an influence from plume between ca. 1.55 Ga to 1.35 Ga, as shown by large igneous provinces in Fennoscandia at ca. 1.50 Ga, 1.46 Ga, 1.41 Ga and 1.38 Ga (Supplementary Table 6, Ernst et al., 2008; Puchkov et al., 2013). Even though such plume signatures exist, the majority of mafic to intermediate rocks (1.6–1.3 Ga) in these three domains are remarkably dominated by arc signatures (Fig. 8c to 8f, Supplementary Table 5). This predominance of magmatism with arc signatures suggests that subduction plays an essential role in causing the breakup of Nuna.

The critical role of subduction on the breakup of Nuna can also be unveiled by compilation of available geological records from blocks in the periphery of Nuna (Laurentia, Eastern Antarctica, West Australia, North China, India and Amazon (Fig. 9a and 10). Around the south-eastern margin of the Laurentia, a 1.8–1.3 Ga accretionary belt exits (Hanmer et al., 2000; Karlstrom et al., 2001; Gower and Krogh, 2002; Whitmeyer and Karlstrom, 2007). Most rocks from this belt are characterized by calc-alkaline compositions and juvenile isotopic signatures, suggesting that these rocks were formed in arc settings (Rivers and Corrigan, 2000; Blein et al., 2003; Bickford et al., 2015; Marshall et al., 2017; Groulier et al., 2018; Maity and Indares, 2018). Their arc affinities have been attributed to the subduction surrounding the Laurentia (Rivers and Corrigan, 2000; Gower and Krogh, 2002; Dickin et al., 2010; Bickford et al., 2015; Rogers et al., 2019). In the Eastern Antarctica, magmatism and metamorphism occurred at 1.5–1.3 Ga, and all reflect an affinity to subduction (Mikhalsky et al., 1996; Liu et al., 2014b, 2016; De Vries Van Leeuwen et al., 2019). Moreover, detrital provenance records calc-alkaline geochemical characteristics of magmatism in the Eastern Antartica, suggesting the development of an accretionary belt in the early to middle Mesoproterozoic (Marschall et al., 2013). Mesoproterozoic rock association in West Australia consists of a series of subduction-related dykes, ophiolites and sediments around 1.55–1.33 Ga (Spaggiari et al., 2015, 2018; Aitken et al., 2016; Maritati et al., 2019), which likewise suggests a subduction complex. In the southern margin of the North China Craton, subduction-related magmatic rocks (1.78–1.45 Ga) are dominated by arc-related basaltic andesites, andesites and felsic rocks (Zhao et al., 2009; He et al., 2010a, 2010b), while the North China Craton was suggested to face an open global ocean at ca.1.4 Ga (Zhang et al., 2019a). Meanwhile, early to middle Mesoproterozoic subduction system can be observed along the periphery of eastern India, where main arc phase, ophiolitic mélange and metamorphism manifested accretionary process (Rogers and Santosh, 2002; Meert et al., 2010; Dharma Rao et al., 2011; Pisarevsky et al., 2013; Hrushikesh et al., 2019; Hazarika et al., 2020). Similarly, successive accretion of magmatic arcs demonstrates a convergent margin around southwest Amazon (Cordani and Teixeira, 2007; Bettencourt et al., 2010; Teixeira et al., 2015). The above lines of evidence indicates that subduction-related records are absent in the interior blocks of Nuna but do occur in the periphery of Nuna (Fig. 9a and 10), which thus suggests a circum-supercontinent subduction along the margin of Nuna (Fig. 10). This circum-supercontinent subduction coincided with Nuna's breakup. It is thus reasonable to suggest that an exterior subduction surrounding the supercontinent plays a great role in the breakup of Nuna (Fig. 10).

5.4.2. External subduction versus plume-related magmatism

Exterior subduction is critical for Nuna's breakup in the early to middle Mesoproterozoic. Meanwhile, it was accompanied by intermittent plume activities in the interiors or landward peripheral blocks of Nuna. During the exterior subduction, large igneous provinces and/or anorogenic magmatism episodically emerged in the inboard blocks of Nuna (Fig. 9a, 10 and supplementary Table 6). They were pervasive and occurred as radial dyke swarms, sills, anorthosite-mangerite-charnockite-granite, A-type granite and rapakivi granite, which reflected anorogenic settings and a plume affinity (Upton et al., 2005; Ernst et al., 2008; Bahat et al., 2013; Shalivahan et al., 2014; Teixeira et al., 2015; Gladkochub et al., 2016; Donskaya et al., 2018). The plume-

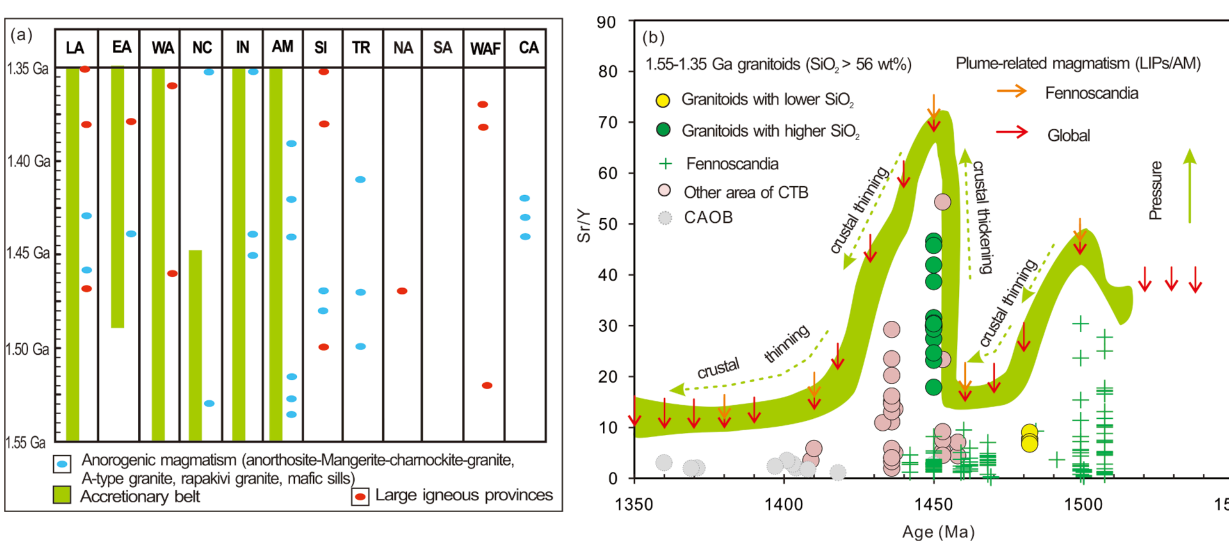

Fig. 9. (a) Compilation of 1.55–1.35 Ga accretionary belts, large igneous provinces and/or anorogenic magmatism (LIPs and/or AM) in the Laurentia (LA) (Upton et al., 2005; Ernst et al., 2008), Eastern Antarctica (EA) (Ernst et al., 2008; Goodge et al., 2010), West Australia (WA) (Ernst et al., 2008), North China (NC) (Zhang et al., 2009; Chen et al., 2013; Deng et al., 2016), India (IN) (Ghodke et al., 2018), Amazon (AM) (Fraga et al., 2009; Bispo-Santos et al., 2012, 2020; D'Agrella-Filho et al., 2012; Heinonen et al., 2012; Teixeira et al., 2015), Siberia (SI) (Ernst et al., 2008, 2016a, 2016b; Gladkochub et al., 2016), Tarim (TR) (Wu et al., 2014; Ye et al., 2016; Wang et al., 2018), North and South Australia (NA and SA) (Ernst et al., 2008), West Africa (WAF) (Ernst et al., 2008; Bahat et al., 2013) and Cathaysia (CA) (Li et al., 2002c, 2008; Zhang et al., 2018c, 2019b). (b) Sr/Y versus age diagram for the felsic magmatism from this study, other area of CTB and CAOB as well as Fennoscandia. It shows that the plume-related magmatism was generated during the crustal thinning, but was rarely obsevered while the crustal thickening. Data is from Supplementary Table 5 and Supplementary Table 6.

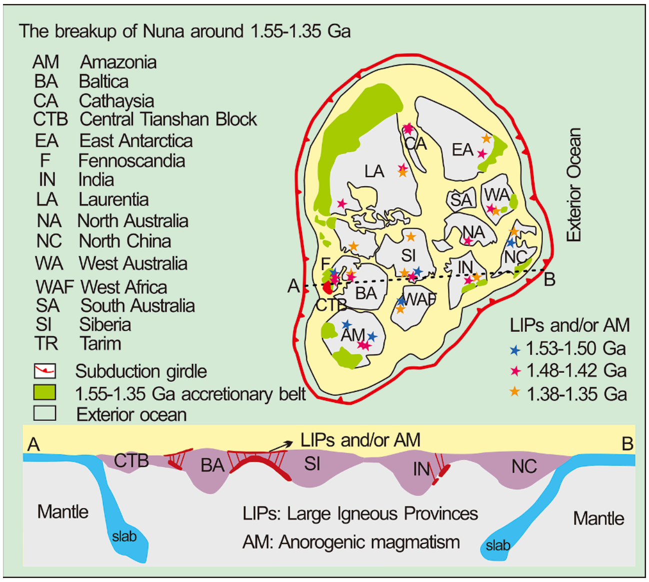

Fig. 10. Schematic model illustrates the dynamic model for breakup of Nuna around 1.55–1.35 Ga. A major exterior subduction system along the margin of Nuna causes Nuna breakup, which was accompanied by subordinate multistage plumes. A-B is the schematic cross section illustrating a dominant process of circum-supercontinent subduction to drive the breakup of Nuna with subordinate intermittent plumes.Compilation data of 1.55–1.35 Ga large igneous provinces and/or anorogenic magmatism are the same as in Fig. 9 and listed in Supplementary Table 6.

related magmatism was temporally linked to the development of exterior subdution around the periphery of Nuna (Fig. 9a and 10), suggesting a coexistent relationship. Although having a plume affinity, these magmatism were overprinted with arc signatures and mostly exhibited transition characteristics between the subduction-related arc signatures and plume-related OIB signatures (Fig. 8c-8f, Supplementary Table 5). The plume is considered to cause lithospheric extension in the interior of Nuna (Bahat et al., 2013; Wu et al., 2014; Gladkochub et al., 2016; Zhang et al., 2018c), while coeval exterior subduction occurred mainly around the periphery of Nuna. Althouth both the exterior subduction and plume could contribute to the breakup of Nuna, whether the two factors functioned independently remains unknown. One school of thoughts suggested that the exterior subduction is the major cause to drive the superpercontinent breakup (e.g., Cawood et al., 2016; Wan et al., 2019). The other suggested that the plume is the prime driving force to fragment the supercontinents (e.g., Zhang et al., 2018b). The difficulty in solving this debate is to establish the geochemical correlation between the exterior subduction and plume, as they are spatially isolated. The plume occurred in the interiors of Nuna, while the exterior subduction happened around the supercontinent margin. In order to solve this problem, global geological data in the early to middle Mesoproterozoic are compiled to place constraints.

Variable dips and velocities of subducting slabs control the geometry of the convergent plate margin (Cawood et al., 2009). Generally, trench retreat characterized by retreating of downgoing slab relative to the overriding plate (e.g., slab rollback) tends to induce crustal thinning, whereas trench advance marked by advancing of overriding plate toward the downgoing slab (e.g., flat subduction) is likely to cause crustal thickening (Collins, 2002; Zhang et al., 2018d). Therefore, tracing the changes in crustal thickness can provide crucial clues for the role of exterior subduction process around the margin of Nuna, which can help define the subduction-plume relationship for the Nuna breakup.

Geochemical indices such as Sr/Y, La/Yb, Dy/Yb, and Ho/Yb of crust-derived felsic rocks can be used to quantify the crustal thickness, as they are sensitive to crustal thickness variations and decrease with decreasing crustal depths (Chapman et al., 2015; Chiaradia, 2015; Zhang et al., 2018d). In this study, we employ Sr/Y ratios of the arc-related granitoids produced by exterior subduction in the CTB-CAOB and Fennoscandia and the variation of Sr/Y ratios with time is illustrated in Fig. 9b. It shows that, during the Mesoproterozoic (1.55 Ga to 1.35 Ga), Sr/Y ratios of the granitoids are highly fluctuant over time (green ribbon in Fig. 9b), reflecting alternated thinning and thickening of the crust, which corresponds to the trench retreat and advance, respectively. The variation in crustal thickness suggests that the breakup of Nuna was not a monotonous process and crustal thinning was interspersed with crustal thickening. The Sr/Y ratios decrease from ca. 1.50 Ga to 1.46 Ga and from ca. 1.45 Ga to 1.35 Ga (Fig. 9b), suggesting two phases of trench retreats. While marking the plume information in the diagram (arrows in Fig. 9b), it is noticed that the plume-related magmatism occurred mostly during the periods when the thickened crust became thinning. This suggests that plume-related magmatism was almost entirely associated with the trench retreat of the exterior subduction. For example, in the period of trench retreats, large igneous provinces in Fennoscandia occurred in ca. 1.50 Ga, 1.46 Ga, 1.41 Ga and 1.38 Ga (Fig. 9b, Supplementary Table 6). Furthermore, in Nuna's interior that was hundreds and thousands kilometers away from exterior subduction zone, global records of Mesoproterozoic plume-related magmatism only appeared in the trench retreat periods (Fig. 9b and Supplementary Table 6). However, the plume-related magmatism was rarely observed during the trench advance leading to crustal thickening at ca. 1.46–1.45 Ga (Fig. 9b). The above facts therefore imply a temporal and geodynamical link between the plume-related magmatism and the exterior subduction with trench retreats. The coupling of plume-related magmatism with the retreating of exterior subduction suggests that the exterior subduction played an initiative role in driving Nuna to breakup, while the process of plume was subordinate. Moreover, the Nuna's assembly was mainly completed in 2.0–1.8 Ga, as has been revealed in the Fennoscandia-CTB which was on the edge of Nuna during its amalgamation (Roberts and Slagstad, 2015). Later than the main stage of Nuna assembly, exterior subduction-related arc magmatism in the Fennoscandia and CTB were emerged at 1.86 Ga and ca. 1.48–1.38 Ga, respectively (Roberts and Slagstad, 2015; Supplementary Table 5). Therefore, it is unlikely for the exterior subduction to contribute to Nuna's assembly. Nevertheless, the exterior subduction can drive the Nuna to break up, as it was initially developed in the outboard Nuna and spanned the lifetime of its breakup. Our observations further support recent geodynamical modeling results and analysis of geological history of Rodinia that exterior subduction can cause internal lithospheric extension in the supercontinetal interior to break up the supercontinent (Cawood et al., 2016; Yang et al., 2018; Dal Zilio et al., 2018).

Therefore, available global geological data unveils a dominant role of exterior subduction operating on the breakup of Nuna with subordinate intermittent plume in the early to middle Mesoproterozoic. The early to middle Mesoproterozoic period was previously believed to be an interval of environmental stasis with tectonic stability (Buick et al., 1995; Brasier and Lindsay, 1998; Holland, 2006; Lyons et al., 2014). Our study suggests that this interval was far more tectonically active than previously thought. This might be the reason that fluctuated atmospheric oxygen concentration was proposed and complex eukaryote life with episodic deposit mineralization were recorded in this period (Goldfarb et al., 2001; Holland, 2006; Leach et al., 2010; Kaur and Chaudhri, 2014; Large et al., 2017; Mukherjee et al., 2018; Zhang et al., 2018a). It is thus recommended that a dominant influence from subduction together with subordinate periodic plume for Nuna breakup should be taken into consideration to understand the environment, life and metallogeny of the early to middle Mesoproterozoic period.

6. Conclusions

1. The Mesoproterozoic granitoids in the CTB are I type granites. Those with lower SiO_2 were formed from partial melting of a hydrous medium-to high K basaltic source in a subduction-related setting,

and differentiated to form those with higher SiO_2 by factional crystallization.

2. The Mesoproterozoic granitoids in the CTB, CAOB and Fennoscandia, which together with the 1.6–1.3 Ga accretionary belts in the peripheral blocks of Nuna, indicate the development of an encircling subduction system surrounding Nuna.
3. Exterior subduction in the periphery of Nuna played a major role in driving the supercontinent to breakup in the early to middle Mesoproterozoic, which was accompanied by subordinate intermittent plume activities. The joint roles of subduction with subordinate plume activities for the breakup of Nuna are most likely to explain oscillatory increase of oxygen level and complex of eukaryote life with episodic deposits formation in the early-middle Mesoproterozoic period.

CRediT authorship contribution statement

Zongying Huang: Conceptualization, Funding acquisition, Investigation, Methodology, Writing - review & editing. **Chao Yuan:** Conceptualization, Validation, Funding acquisition, Supervision, Writing - review & editing. **Xiaoping Long:** Resources, Supervision. **Yunying Zhang:** Investigation, Writing - review & editing. **Xiaolong Ma:** Formal analysis, Writing - review & editing. **Jérémie Soldner:** Investigation, Formal analysis. **Long Du:** Investigation. **Chutian Shu:** Investigation.

Declaration of Competing Interest

The authors declare that they have no known competing financial interests or personal relationships that could have appeared to influence the work reported in this paper.

Acknowledgements

We would like to thank two reviewers and the editor for their constructive comments, which help improve the manuscript. This study is supported by the Natural Science Foundation of China (418030304, 41973021 and 42021002). HUANG ZY acknowledges the financial support of the Guangzhou Science and Technology Program: Basic and Applied Basic Research Project (202102020418) during the research. This work is also fund by National Key Research and Development Program of China (2017YFC0601205 and 2019YFA0708601), the International Partnership Program of Chinese Academy of Sciences (132744KYSB20190039 and 132744KYSB20200001) and the China Postdoctoral Science Foundation Grant (2018M633171). Presented data used in this study are available in the figures and the references and supplemental materials.

Appendix A. Supplementary data

Supplementary data to this article can be found online at https://doi.org/10.1016/j.precamres.2021.106287.

References

Åhäll, K.I., Connelly, J.N., 2008. Long-term convergence along SW Fennoscandia: 330 m.y. of Proterozoic crustal growth. Precambr. Res. 161 (3–4), 452–474. https://doi.org/10.1016/j.precamres.2007.09.007.

Aitken, A.R.A., Betts, P.G., Young, D.A., Blankenship, D.D., Roberts, J.L., Siegert, M.J., 2016. The Australo-Antarctic Columbia to Gondwana transition. Gondwana Res. 29 (1), 136–152. https://doi.org/10.1016/j.gr.2014.10.019.

Andersen, T., Griffin, W.L., Jackson, S.E., Knudsen, T.-L., Pearson, N.J., 2004. Mid-Proterozoic magmatic arc evolution at the southwest margin of the Baltic Shield. Lithos 73 (3-4), 289–318. https://doi.org/10.1016/j.lithos.2003.12.011.

Andersson, U.B., 1997. The sub-Jotnian strömsbro granite complex at gävle, Sweden. GFF 119 (2), 159–167. https://doi.org/10.1080/11035899709546473.

Bahat, A.E., Ikenne, M., Söderlund, U., Cousens, B., Youbi, N., Ernst, R., Soulaimani, A., Janati, M.I., Hafid, A., 2013. U-Pb baddeleyite ages and geochemistry of dolerite dykes in the Bas Drâa Inlier of the Anti-Atlas of Morocco: Newly identify 1380 Ma event in the West African Craton. Lithos 174, 85–98. https://doi.org/10.1016/j.lithos.2012.07.022.

Banno, S., Higashino, T., Otsuki, M., Itaya, T., Nakajima, T., 1978. Thermal structure of the Sanbagawa metamorphic belt in Central Shikoku. J. Phy. Earth 26, 345–356. https://doi.org/10.4294/jpe1952.26.

Bercovici, D., Long, M.D., 2014. Slab rollback instability and supercontinent dispersal. Geophys. Res. Lett. 41 (19), 6659–6666. https://doi.org/10.1002/2014GL061251.

Bettencourt, J.S., Leite, W.B., Ruiz, A.S., Matos, R., Payolla, B.L., Tosdal, R.M., 2010. The Rondonian-San Ignacio Province in the SW Amazonian Craton. An overview. J. South Am. Earth Sci. 29 (1), 28–46. https://doi.org/10.1016/j.jsames.2009.08.006.

Bickford, M.E., Van Schmus, W.R., Karlstrom, K.E., Mueller, P.A., Kamenov, G.D., 2015. Mesoproterozoic-trans-Laurentian magmatism. A synthesis of continent-wide age distributions, new SIMS U-Pb ages, zircon saturation temperatures, and Hf and Nd isotopic compositions. Precambr. Res. 265, 286–312. https://doi.org/10.1016/j.precamres.2014.11.024.

Bingen, B., Viola, G., 2018. The early-Sveconorwegian orogeny in southern Norway: Tectonic model involving delamination of the sub-continental lithospheric mantle. Precambr. Res. 313, 170–204. https://doi.org/10.1016/j.precamres.2018.05.025.

Bispo-Santos, F., D`Agrella-Filho, M.S., Pesonen, L.J., Salminen, J.M., Reis, N.J., Silva, J. M., 2020. The long life of SAMBA connection in Columbia: A paleomagnetic study the 1535 Ma Mucajai Complex, north Amazonian Craton, Brazil. Gondwa Res. 196–197, 1–22. https://doi.org/10.1016/j.gr.2019.09.016.

Bispo-Santos, F., D'Agrella-Filho, M.S., Trindade, R.I.F., Elming, S.A., Janikian, L., Vasconcelos, P.M., Perillo, B.M., Pacca, I.G., Silva, J.A., Barros, M.A.S., 2012. Tectonic implications of the 1419 Ma Nova Guarita mafic intrusives paleomagnetic pole (amazonian craton) on the longevity of Nuna. Precambr. Res. 196–197, 1–22. https://doi.org/10.1016/j.precamres.2011.10.022.

Blein, O., LaFlèche, M.R., Corriveau, L., 2003. Geochemistry of the granulitic Bondy gneiss complex: A 1.4 Ga arc in the Central Metasedimentary Belt, Grenville Province, Canada. Precambr. Res. 120, 193–217. https://doi.org/10.1016/S0301-9268(02)00112-2.

Boehnke, P., Watson, E.B., Trail, D., Harrison, T.M., Schmitt, A.K., 2013. Zircon saturation re-visited. Chem. Geol. 351, 324–334. https://doi.org/10.1016/j.chemgeo.2013.05.028.

Bonin, B., 2007. A-type granites and related rocks: evolution of a concept, problems and prospects. Lithos 97 (1–2), 1–29. https://doi.org/10.1016/j.lithos.2006.12.007.

Bouvier, A., Vervoort, J.D., Patchett, P.J., 2008. The Lu–Hf and Sm–Nd isotopic composition of CHUR: Constraints from unequilibrated chondrites and implications for the bulk composition of terrestrial planets. Earth Planet. Sci. Lett. 273 (1-2), 48–57. https://doi.org/10.1016/j.epsl.2008.06.010.

Brander, L., Söderlund, U., 2009. Mesoproterozoic (1.47–1.44 Ga) orogenic magmatism in Fennoscandia; baddeleyite U-Pb dating of a suite of massif-type anorthosite in S Sweden. Inte. J. Earth Sci. 98, 499–516. https://doi.org/10.1007/s00531-007-0281-0.

Brandl, P.A., Regelous, M., Beier, C., Haase, K.M., 2013. High mantle temperatures following rifting caused by continental insulation. Nat. Geosci. 6 (5), 391–394. https://doi.org/10.1038/ngeo1758.

Bradley, D.C., 2011. Secular trends in the geologic record and the supercontinent cycle. Earth Sci. Rev. 108 (1-2), 16–33. https://doi.org/10.1016/j.earscirev.2011.05.003.

Brasier, M.D., Lindsay, J.F., 1998. A billion years of environmental stability and the emergence of eukaryotes: new data from northern Australia. Geology 26, 555–558. https://doi.org/10.1130/0091-7613(1998)026<0555:ABYOES>2.3.CO;2.

Brown, M., 1998. Unpairing metamorphic blets: P-T paths and tectonic model for the Ryoke Belt, southwestern Japan. J. Metamorph. Geol. 16, 3–22. https://doi.org/10.1111/j.1525-1314.1998.00061.x.

Buick, R., Des Marais, D.J., Knoll, A.H., 1995. Stable isotopic compositions of carbonates from the Mesoproterozoic Bangemall Group, northwestern Australia. Chem. Geol. 123 (1-4), 153–171. https://doi.org/10.1016/0009-2541(95)00049-R.

Burov, E., Gerya, T., 2014. Asymmetric three-dimensional topography over mantle plumes. Nature 513 (7516), 85–89. https://doi.org/10.1038/nature13703.

Collins, W.J., Murphy, J.B., Johnson, T.E., Huang, H.Q., 2020. Critical role of water in the formation of continental crust. Nat. Geosci. 13 (5), 331–338. https://doi.org/10.1038/s41561-020-0573-6.

Campbell, I.H., 2007. Testing the plume theory. Chem. Geol. 241 (3–4), 153–176. https://doi.org/10.1016/j.chemgeo.2007.01.024.

Campbell, I.H., 2001. Identification of ancient mantle plumes. Geol. Soci. Am. 352, 5–21. https://doi.org/10.1130/0-8137-2352-3.5.

Cawood, P.A., Hawkesworth, C.J., 2014. Earth's middle age. Geology 42, 503–506. https://doi.org/10.1130/G35402.1.

Cawood, P.A., Hawkesworth, C.J., 2015. Temporal relations between mineral deposits and global tectonic cycles: implications for prospectivity: In Jenkin, G.R.T., Lusty, P. A.J., McDonald, I., Smith, M.P., Boyce, A.J. & Wilkinson, J.J. (Eds.) Ore Deposits in an Evolving Earth. Geol. Soci. Lon. Special Publications 393, 9–21, https://doi.org/10.1144/sp393.1.

Cawood, P.A., Kröner, A., Collins, W.J., Kusky, T.M., Mooney, W.D., Windley, B.F., 2009. Accretionary orogens through Earth history, in Earth Accretionary Systems in Space and Time, edited by P.A. Cawood and A. Kröner. Geological Society of London, Special Publication, 318 (1), 1–36.

Cawood, P.A., Strachan, R.A., Pisarevsky, S.A., Gladkochub, D.P., Murphy, J.B., 2016. Linking collisional and accretionary orogens during Rodinia assembly and breakup: Implication for models of supercontinent cycles. Earth Planet. Sci. Lett. 449, 118–126. https://doi.org/10.1016/j.epsl.2016.05.049.

Chappell, B.W., 1999. Aluminium saturation in I- and S-type granites and the characterization of fractionated haplogranites. Lithos 46 (3), 535–551. https://doi.org/10.1016/S0024-4937(98)00086-3.

Čečys, A., Bogdanova, S., Janson, C., Bibikova, E., Kornfält, K.A., 2002. The Stenshuvud and Tåghusa granitoids: new representatives of Mesoproterozoic magmatism in southern Sweden. GFF 124 (3), 149–162. https://doi.org/10.1080/11035890201243149.

Černý, P., Teertstra, D.K., Chapman, R., Selway, J.B., Hawthorne, F.C., Ferreira, K., Chackowsky, L.E., Wang, X.-J., Meintzer, R.E., 2012. Extreme fractionation and deformation of the leucogranite-pegmatite suite at Red Cross Lake, Manitoba, Canada. IV. Mineral. Can. Mineral. 50 (6), 1839–1875. https://doi.org/10.3749/canmin.50.6.1839.

Chapman, J.B., Ducea, M.N., DeCelles, P.G., Profeta, L., 2015. Geology Tracking changes in crustal thickness during orogenic evolution with Sr/Y An example from the North American Cordillera. Geology 43 (10), 919–922.

Chappell, B.W., Stephens, W.E., 1988. Origin of infracrustal (I-type) granite magmas. Trans. R. Soc. Edinburgh Earth Sci. 79 (2-3), 71–86. https://doi.org/10.1017/S0263593300014139.

Chappell, B.W., White, A.J.R., 1974. Two contrasting granite types. Pac. Geol. 8, 173–174.

Chappell, B.W., White, A.J.R., 1992. I- and S-type granites in the Lachlan Fold Belt. Trans. R. Soc. Edinburgh Earth Sci. 83 (1-2), 1–26. https://doi.org/10.1017/S0263593300007720.

Charvet, J., Shu, L.S., Laurent-Charvet, S., 2007. Paleozoic structural and geodynamic evolution of eastern Tianshan (NW China): welding of the Tarim and Junggar plates. Episodes 30, 162–186. https://hal-insu.archives-ouvertes.fr/insu-00179631.

Chen, L.W., Huang, B.C., Yi, Z.Y., Zhao, J., Zhao, J., Yan, Y.G., 2013. Paleomagnetism of ca. 1.35 Ga sills in northern North China Craton and implications for paleogeographic reconstruction of the Mesoproterozoic supercontinent. Precambr. Res. 228, 36–47. https://doi.org/10.1016/j.precamres.2013.01.011.

Chiaradia, M., 2015. Crustal thickness control on Sr/Y signatures of recent arc magmas: An Earth scale perspective. Sci. Rep. 5, 8115.

Chudík, P., Uher, P., Kohút, M., Bačík, P., 2008. Accessory columbite totantalite, tapiolite and zircon: Products of extreme fractionation in highly peraluminous pegmatitic granite from the Považský Inovec Mountains, Western Carpathians, Slovakia. J. Geosci. 53, 323–334. https://doi.org/10.3190/jgeosci.031.

Claesson, S., Kresten, P., 1997. The anorgenic Noran intrusion-a Mesoproterozoic rapakivi massif in south-central Sweden. GFF 119, 115–122. https://doi.org/10.1080/11035899709546466.

Clemens, J.D., Stevens, G., 2012. What controls chemical variation in granitic magmas? Lithos 134–135, 317–329. https://doi.org/10.1016/j.lithos.2012.01.001.

Clemens, J.D., Holloway, J.R., White, A.J.R., 1986. Origin of an A-type granite: experimental constraints. Am. Miner. 71, 317–324. http://www.minsocam.org/ammin/AM71/AM71_317.pdf.

Clemens, J.D., Stevens, G., Farina, F., 2011. The enigmatic sources of I-type granites: The peritectic connexion. Lithos 126 (3-4), 174–181. https://doi.org/10.1016/j.lithos.2011.07.004.

Collins, W.J., 2002. Hot orogens, tectonic switching, and creation of continental crust. Geology 30 (6), 535–538. https://doi.org/10.1130/0091-7613(2002)030<0535:HOTSAC>2.0.CO;2.

Cordani, U.G., Teixeira, W., 2007. Proterozoic accretionary belts in the Amazonina Craton. Geol. Soc. Am. Men. 200, 297–320. https://doi.org/10.1130/2007.1200(14).

D'Agrella-Filho, M.S., Trindade, R.I.F., Elming, S.Å., Teixeira, W., Yokoyama, E., Tohver, E., Geraldes, M.C., Pacca, I.I.G., Barros, M.A.S., Ruiz, A.S., 2012. The 1420 Ma Indiavaí Mafic Intrusion (SW Amazonian Craton): paleomagnetic results and implications for the Columbia Supercontinent. Gondwana Res. 22, 956–973. https://doi.org/10.1016/j.gr.2012.02.022.

Dal Zilio, L., Faccenda, M., Capitanio, F., 2018. The role of deep subduction in supercontinent breakup. Tectonophysics 746, 312–324. https://doi.org/10.1016/j.tecto.2017.03.006.

Davidson, J., Turner, S., Handley, H., Macpherson, C., Dosseto, A., 2007. Amphibole "sponge" in arc crust. Geology 35 (9), 787. https://doi.org/10.1130/G23637A.110.1130/2007196.

De Vries Van Leeuwen, A.T., Morrissey, L.J., Kelsey, D.E., Raimondo, T., 2019. Recognition of Pan-African-aged metamorphism in the Fisher Terrane, central Prince Charles Mountains, East Antarctica. J. Geol. Soci. 176 (4), 785–798. https://doi.org/10.1144/jgs2018-146.

Deng, X.Q., Zhao, T.P., Peng, T.P., 2016. Age and geochemistry of the early Mesoproterozoic A-type granites in the southern margin of the North China Craton: Constraints on their petrogenesis and tectonic implications. Precambr. Res. 283, 68–88. https://doi.org/10.1016/j.precamres.2016.07.018.

Dickin, A.P., McNutt, R.H., Martin, C., Guo, A., 2010. The extent of juvenile crust in the Grenville Province: Nd isotope evidence. Geol. Soc. Am. Bull. 122 (5-6), 870–883. https://doi.org/10.1130/B26381.1.

Dilek, Y., Furnes, H., 2011. Ophiolite genesis and global tectonics: Geochemical and tectonic fingerprinting of ancient oceanic lithosphere. Geol. Soc. Am. Bull. 123 (3-4), 387–411. https://doi.org/10.1130/B30446.110.1130/2011131.

Donskaya, T.V., Gladkochub, D.P., Ernst, R.E., Pisarevsky, S.A., Mazukabzov, A.M., Demonterova, E.I., 2018. Geochemistry and petrogenesis of Mesoproterozoic dykes of the Irkutsk Promontory, Southern part of the Siberian Craton. Miner. 8, 545. https://doi.org/10.3390/min8120545.

Doucet, L.S., Li, Z.X., Ernst, R.E., Kirscher, U., Dien EI, H.G., Mitchell, R.N., 2019. Coupled supercontinent-mantle plume events evidenced by oceanic plume record. Geology 2, 159–163. https://doi.org/10.1130/G46754.1.

Ducea, M.N., Saleeby, J.B., Bergantz, G., 2015. The architecture, chemistry, and evolution of continental magmatic arcs. Annu. Rev. Earth Planet. Sci. 43, 299–331. https://doi.org/10.1046/annurew-earth-060614-105049.

Dharma Rao, C.V., Santosh, M., Wu, Y.B., 2011. Mesoproterozoic ophiolitic mélange from the SE periphery of the Indian plate: U/Pb zircon ages and tectonic implications. Gondwana Res. 19, 384–401. https://doi.org/10.1016/j.gr.2010.06.007.

Eby, G., 1992. Chemical subdivision of the A-type granitoids: Petrogenetic and tectonic implication. Geology 20, 641–644. https://doi.org/10.1130/0091-7613(1992)020<0641:CSOTAT>2.3.CO;2.

Ernst, R.E., Buchan, K.L., 2003. Recognizing mantle plumes in the geological record. Annu. Rev. Earth Planet. Sci. 31, 469–523. https://doi.org/10.1146/annurev.earth.31.100901.145500.

Ernst, R.E., Hamilton, M.A., Söderlund, U., Hanes, J.A., Gladkochub, D.P., Okrugin, A.V., Kolotilina, T., Mekhonoshin, A.S., Bleeker, W., LeCheminant, A.N., Buchan, K.L., Chamberlain, K.R., Didenko, A.N., 2016a. Long-lived connection between southern Siberia and northern Laurentia in the Proterozoic. Nat. Geosci. https://doi.org/10.1038/NGEO2700.

Ernst, R.E., Okrugin, A.V., Veselovskiy, R.V., Kamo, S.L., Hamilton, M.A., Pavlov, V., Söderlund, U., Chamberlain, K.R., Rogers, C., 2016b. The 1501 Ma Kuonamka Large Igneous Province of northern Siberia: U-Pb geochronology, geochemistry, and links with coeval magmatism on other crustal blocks. Russ. Geol. Geophys. 57, 653–671. https://doi.org/10.1016/j.rgg.2016.01.015.

Ernst, R.E., Wingate, M.T.D., Buchan, K.L., Li, Z.X., 2008. Global record of 1600–700 Ma Large Igneous Provinces (LIPs): Implications for the reconstruction of the proposed Nuna (Columbia) and Rodinia supercontinents. Precambr. Res. 160 (1-2), 159–178. https://doi.org/10.1016/j.precamres.2007.04.019.

Ernst, W.G., 2005. Alpine and Pacific styles of Phanerozoic mountain building: subduction-zone petrogenesis of continental crust. Terra Nova 17, 165–188. https://doi.org/10.1111/j.1365-3121.2005.00604.x.

Evans, D.A.D., Mitchell, R.N., 2011. Assembly and breakup of the core of Paleoproterozoic-Mesoproterozoic supercontinent Nuna. Geology 39 (5), 443–446. https://doi.org/10.1130/G31654.110.1130/2011145.

Fraga, L.M.B., Dall'Agnol, R., Costa, J.B.S., Macambira, M.J.B., 2009. The Mesoproterozoic Mucajai anorthosite–mangerite–rapakivi granite complex, Amazonian Craton. Brazil. Can. Miner. 47, 1469–1492. https://doi.org/10.3749/canmin.47.6.1469.

Ewart, A., Bryan, W.B., Gill, J.B., 1973. Mineralogy and Geochemistry of the Younger Volcanic Islands of Tonga. S. W. Pacific. J. Petrol. 14, 429–465.

Frost, B.R., Barnes, C.G., Collins, W.J., Arculus, R.J., Ellis, D.J., Frost, C.D., 2001. A geochemical classifcation for granitic rocks. J. Petrol. 42, 2033–2048. https://doi.org/10.1093/petrology/42.11.2033.

Frost, C.D., Frost, B.R., 2011. On ferroan (A-type) granitoids: their compositional variability and modes of origin. J. Petrol. 52 (1), 39–53. https://doi.org/10.1093/petrology/egq070.

Frost, C.D., Frost, B.R, Beard, J.S., 2016. On silica-rich granitoids and their eruptive equivalents. Am. Miner. 101 (6), 1268–1284. https://doi.org/10.2138/am-2016-5307.

Gao, J., Long, L.L., Klemd, R., Qian, Q., Liu, D.Y., Xiong, X.M, Su, W., Liu, W., Wang, Y.T., Yang, F.Q., 2009. Tectonic evolution of the South Tianshan orogen and adjacent regions, NW China: geochemical and a geconstraints of granitoid rocks. Int. J. Earth Sci. 98 (6), 1221–1238. https://doi.org/10.1007/s00531-008-0370-8.

Gao, P., Lu, Y.H., Zhao, Z.F., Zheng, Y.F., 2020. The composition variation of I-type granites: Constraints from geochemical analyses and phase equilibrium calculations for granites from the Qinling orogen, central China. J. Asian Earth Sci. 200, 104471 https://doi.org/10.1016/j.jseaes.2020.104471.

Gelman, S.E., Deering, C.D., Bachmann, O., Huber, C., Gutiérrez, F.J., 2014. Identifying the crystal graveyards remaining after large silicic eruptions. Earth Planet. Sci. Lett. 403, 299–306. https://doi.org/10.1016/j.epsl.2014.07.005.

Ghodke, S.S., Rathna, K., Kokandakar, G.J., Nagaraju, B., More, L.B., Bhosle, M.V., Kumar, B.K., 2018. Emplacement and growth of alkaline dikes: Insights from the shonkinite dikes (Elchuru alkaline complex, SE India). J. Struct. Geol. 117, 219–236. https://doi.org/10.1016/j.jsg.2018.09.016.

Gladkochub, D.P., Donskaya, T.V., Mazukabzov, A.M., Pisarevsky, S.A., Ernst, R.E., Stanevich, A.M., 2016. The Mesoproterozoic mantle plume beneath the northern part of the Siberian craton. Russ. Geol. Geophys. 57, 672–686. https://doi.org/10.1016/j.rgg.2016.04.004.

Goldfarb, R.J., Groves, D.I., Gardoll, S., 2001. Orogenic gold and geologic time: A global synthesis. Ore Geol. Rev. 18 (1–2), 1–75. https://doi.org/10.1016/S0169-1368(01)00016-6.

Goodge, J.W., Fanning, C.M., Brecke, D.M., Licht, K.J., Palmer, E.F., 2010. Continuation of the Laurentian Grenville province across the Ross Sea margin of East Antarctica. J. Geol. 118 (6), 601–619. https://doi.org/10.1086/656385.

Gower, C.F., Krogh, T.E., 2002. A U-Pb geochronological review of the Proterzoic history of the eastern Grenville Province. Can. J. Earth Sci. 39, 795–829. https://doi.org/10.1139/E01-090.

Griffin, W.L., Belousova, E.A., Shee, S.R., Pearson, N.J., O'Reilly, S.Y., 2004. Archean crustal evolution in the northern Yilgarn Craton: U-Pb and Hf-isotope evidence from detrital zircons. Precambr. Res. 131 (3-4), 231–282. https://doi.org/10.1016/j.precamres.2003.12.011.

Griffin, W.L., Wang, X., Jackson, S.E., Pearson, N.J., O'Reilly, S.Y., Xu, X.S., Zhou, X.M., 2002. Zircon chemistry and magma mixing, SE China in-situ analysis of Hf isotopes, Tonglu and Pingtan igneous complexes. Lithos 61, 237–269. https://doi.org/10.1016/S0024-4937(02)00082-8.

Groulier, P.A., Indares, A., Dunning, G., Moukhsil, A., Wälle, M., 2018. Peri-Laurentian, Pinwarian-age oceanic arc crust preserved in the Grenville Province: Insights from the Escoumins supracrustal belt. Precambr. Res. 311, 37–64. https://doi.org/10.1016/j.precamres.2018.04.001.

Grove, T.L., Till, C.B., Krawczynski, M.J., 2012. The role of H2O in subduction zone magmatism: Annu. Rev. Earth Planet. Sci. 40, 413–439. https://doi.org/10.1146/annurev-earth-042711-105310.
Han, J., Zhou, J.B., Li, L., Song, M.C., 2017. Mesoproterozoic (~1.4 Ga) A-type gneissic granites in the Xilinhot terrane, NE China: First evidence for the break-up of Columbia in the eastern CAOB. Precambr. Res. 296, 20–38. https://doi.org/10.1016/j.precamres.2017.04.043.
Han, Y.G., Zhao, G.C., Cawood, P.A., Sun, M., Liu, Q., Yao, J.L., 2019. Plume-modification collision orogeny: The Tarim-western Tianshan example in Central Asia. Geology 47. https://doi.org/10.1130/G46855.1.
Hanmer, S., Corrigan, D., Pehrsson, S., Nadeau, L., 2000. SW Grenville Province, Canada: the case against post-1.4 Ga accretionary tectonics. Tectonophysics 319 (1), 33–51. https://doi.org/10.1016/S0040-1951(99)00317-0.
Hanson, G.N., 1978. The application of trace elements to the petrogenesis of igneous rocks of granitic composition. Earth Planet. Sci. Lett. 38 (1), 26–43. https://doi.org/10.1016/0012-821X(78)90124-3.
Harnois, L., 1988. The CIW index: A new chemical index of weathering. Sed. Geol. 55 (3–4), 319–322. https://doi.org/10.1016/0037-0738(88)90137-6.
Hazarika, B., Malpe, D.B., Ashish, D., 2020. Petrogenesis of mafic dykes from the western Bastar craton of Central India and their relation to outgrowth of Columbia supercontinent. Miner. Petrol. 114, 243–262. https://doi.org/10.1007/s00710-020-00695-y.
He, Y.H., Zhao, G.C., Sun, M., 2010a. Geochemical and isotopic study of the Xiong'er volcanic rocks at the southern margin of the North China Craton: Petrogenesis and tectonic implications. J. Geol. 118, 417–433. https://doi.org/10.1086/652733.
He, Y.H., Zhao, G.C., Sun, M., Han, Y., 2010b. Petrogenesis and tectonic setting of volcanic rocks in the Xiaoshan and Waifangshan areas along the southern margin of the North China Craton: Constraints from bulk-rock geochemistry and Sr-Nd isotopic composition. Lithos 114, 186–199. https://doi.org/10.1016/j.lithos.2009.08.008.
He, Z.Y., Klemd, R., Yan, L.L., Zhang, Z.M., 2018. The origin and crustal evolution of microcontinents in the Beishan orogen of the southern Central Asian Orogenic Belt. Earth Sci. Rev. 185, 1–14. https://doi.org/10.1016/j.earscirev.2018.05.012.
He, Z.Y., Klemd, R., Zhang, Z.M., Zong, K.Q., Sun, L.X., Tian, Z.L., Huang, B.T., 2015a. Mesoproterozoic continental arc magmatism and crustal growth in the eastern Central Tianshan Arc Terrane of the southern Central Asian Orogenic Belt: Geochronological and geochemical evidence. Lithos 236–237, 74–89. https://doi.org/10.1016/j.lithos.2015.08.009.
He, Z.Y., Sun, L.X., Mao, L.J., Zong, K.Q., Zhang, Z.M., 2015b. Zircon U-Pb and Hf isotopic study of the gneiss and granodiorite from the southern Beishan orogenic collage: Mesoproterozoic magmatism and crustal growth. Chin.e Sci Bull. 60, 389–399. https://doi.org/10.1360/N972014-00898.
Heinonen, A.P., Fraga, L.M., Rämö, O.T., Dall'Agnol, R., Mänttäri, I., Andersen, T., 2012. Petrogenesis of the igneous Mucajaí AMG complex, northern Amazonian craton geochemical, UePb geochronological, and Nd–Hf–O isotopic constraints. Lithos 151, 17–34. https://doi.org/10.1016/j.lithos.2011.07.016.
Herzberg, C., O'Hara, M.J., 2002. Plume-associated ultramafic magmas of Phanerozoic age. J. Petrol. 43, 1857–1883. https://doi.org/10.1093/petrology/43.10.1857.
Hill, R.I., 1991. Starting plumes and continental break-up. Earth Planet. Sci. Lett. 104 (2–4), 398–416. https://doi.org/10.1016/0012-821X(91)90218-7.
Holland, H.D., 2006. The oxygenation of the atmosphere and oceans. Philos. Trans. R. Soci. B 361 (1470), 903–915. https://doi.org/10.1098/rstb.2006.1838.
Hooper, P.R., 1990. The timing of crustal extension and the eruption of continental flood basalts. Nature 345 (6272), 246–249. https://doi.org/10.1038/345246a0.
Hoskin, P.W., Schaltegger, U., 2003. The composition of zircon and igneous and metamorphic petrogenesis. Rev. Miner. Geochem. 53, 27–62. https://doi.org/10.2113/0530027.
Hou, G.T., Santosh, M., Qian, X., Lister, G.S., Li, J.H., 2008. Tectonic constraints on 1.3–1.2 Ga final breakup of Columbia supercontinent from a giant radiating dyke swarm. Gondwana Res. 14, 561–566. https://doi.org/10.1016/j.gr.2008.03.005.
Hrushikesh, H., Prabhakar, N., Bhattacharya, A., 2019. Mesoproterozoic P-T-t-d history in the Vinjamuru domain, Nellore schist belt (SE India), and implications for SE India-East Antarctica correlation. Precambr. Res. 327, 273–295. https://doi.org/10.1016/j.precamres.2019.04.002.
Hu, A.Q., Wei, J.G., Deng, W.F., Zhang, J.B., Chen, L.L., 2006. 1.4 Ga SHRIMP U-Pb age for zircons of granodiorite and its geological signficance from the eastern segment of the Tianshan Mountains, Xinjiang, China. Geochem. 35, 333–345 (in Chinese with English abstract).
Huang, B.T., He, Z.Y., Zong, K.Q., Zhang, Z.M., 2014. Zircon U-Pb and Hf isotopic study of Neoproterozoic granitic gneisses from the Alatage area, Xinjiang: Constraints on the Precambrian crustal evolution in the Central Tianshan Block. Chin. Sci. Bull. 59 (1), 100–112. https://doi.org/10.1007/s11434-013-0010-y.
Huang, B.T., He, Z.Y., Zhang, Z.M., Klemd, R., Zong, K.Q., Zhao, Z.D., 2015. Early Neoproterozoic granitic gneisses in the Chinese Eastern Tianshan: Petrogenesis and tectonic implications. J. Asian Earth Sci. 113, 339–352. https://doi.org/10.1016/j.jseaes.2014.08.021.
Huang, F., Lundstrom, C., Mcdonough, W., 2006. Effect of melt structure on trace-element partitioning between clinopyroxene and silicic, alkaline, aluminous melts. Am. Miner. 91, 1385–1400. https://doi.org/10.2138/am.2006.1909.
Huang, Z.Y., Long, X.P., Wang, X.C., Zhang, Y.Y., Du, L., Yuan, C., Xiao, W.J., 2017. Precambrian evolution of the Chinese Central Tianshan Block: Constraints on its tectonic affinity to the Tarim Craton and responses to supercontinental cycles. Precambr. Res. 295, 24–37. https://doi.org/10.1016/j.precamres.2017.04.014.
Huang, Z.Y., Yuan, C., Long, X.P., Zhang, Y.Y., Du, L., 2019. From breakup of Nuna to assembly of Rodinia: A link between the Chinese Central Tianshan Block and Fennoscandia. Tectonics 38 (12), 4378–4398. https://doi.org/10.1029/2018TC005471.
Jackson, S.E., Pearson, N.J., Griffin, W.L., Belousova, E.A., 2004. The application of laser ablation-inductively coupled plasma-mass spectrometry to in situ U-Pb zircon geochronology. Chem. Geol. 211 (1–2), 47–69. https://doi.org/10.1016/j.chemgeo.2004.06.017.
Jahn, B.M., Wu, F.Y., Chen, B., 2000. Massive granitoids generation in Central Asia: Nd isotope evidence and implication for continental growth in the Phanerozoic. Episodes 23, 82–92. https://doi.org/10.18814/epiiugs/2000/v23i2/001.
Johansson, Å., Waight, T., Andersen, T., Simonsen, S.L., 2016. Geochemistry and petrogenesis of Mesoproterzoic A-type granitoids from the Danish island of Bornholm, southern Fennoscandia. Lithos 244, 94–108. https://doi.org/10.1016/j.lithos.2015.11.031.
Karlstrom, K.E., Åhäll, K.I., Harlan, S.S., Williams, M.L., McLelland, J., Geissman, J.W., 2001. Long-lived (1.8–1.0 Ga) convergent orogen in southern Laurentia, its extensions to Australia and Baltica, and implications for refining Rodinia. Precambr. Res. 111 (1–4), 5–30. https://doi.org/10.1016/S0301-9268(01)00154-1.
Kaur, P., Chaudhri, N., 2014. Metallogeny associated with the Palaeo-Mesoproterozoic Columbia supercontinent cycle: A synthesis of major metallic deposits. Ore Geol. Rev. 56, 415–422. https://doi.org/10.1016/j.oregeorev.2013.03.005.
Kelemen, P.B., Hanghøj, K., Greene, A., 2003. One view of the geochemistry of subduction-related magmatic arcs, with an emphasis on primitive andesite and lower crust. In: Holland, H.D., Turekian, K.K. (Eds.), Treatise on Geochemistry, Volume 3: Oxford. Elsevier, pp. 593–659.
Kelemen, P.B., Hanghoj, K., Greene, A.R., 2014. One view of the geochemistry of subduction-related magmatic arcs, with an emphasis on primitive andesite and lower crust. Treatise Geochem. 4, 749–805.
Kröner, A., Alexeiev, D.V., Rojas-Agramonte, Y., Hegner, E., Wong, J., Xia, X., Belousova, E., Mikolaichuk, A.V., Seltmann, R., Liu, D., Kiselev, V.V., 2013. Mesoproterozoic (Grenville-age) terranes in the Kyrgyz North Tianshan: Zircon ages and Nd–Hf isotopic constraints on the origin and evolution of basement blocks in the southern Central Asian Orogen. Gondwana Res. 23 (1), 272–295. https://doi.org/10.1016/j.gr.2012.05.004.
Large, R.R., Mukherjee, I., Gregory, D.D., Steadman, J.A., Maslennikov, V.V., Meffre, S., 2017. Ocean and atmosphere geochemical proxies derived from trace elements in marine pyrite: Implications for ore genesis in sedimentary basins. Econ. Geol. 112 (2), 423–450.
Leach, D.L., Bradley, D.C., Huston, D., Pisarevsky, S.A., Taylor, R.D., Gardoll, S.J., 2010. Sediment-hosted lead-zinc deposits in earth history. Econ. Geol. 105, 593–625. https://doi.org/10.2113/gsecongeo.105.3.593.
Lee, C.A., Morton, D.M., Kistler, R.W., Baird, A.K., 2007. Petrology and tectonics of Phanerozoic continent formation: From island arcs to accretion and continental arc magmatism. Earth Planet. Sci. Lett. 263 (3–4), 370–387. https://doi.org/10.1016/j.epsl.2007.09.025.
Li, J., Huang, X.L., He, P.L., Li, W.X., Yu, Y., Chen, L., 2015. In situ analyses of micas in the Yashan granite, South China: Constraints on magmatic and hydrothermal evolutions of W and Ta-Nb bearing granites. Ore Geol. Rev. 65, 793–810. https://doi.org/10.1016/j.oregeorev.2014.09.028.
Li, L., Xiong, X.L., Liu, X.C., 2017. Nb/Ta Fractionation by amphibole in hydrous basaltic systems: implications for arc magma evolution and continental crust formation. J. Petrol. 58, 3–28. https://doi.org/10.1093/petrology/egw070.
Li, Q., Yu, H.F., Xiu, Y.Q., 2002a. On Precambrian basement of the Eastern Tianshan Mountains, Xingjiang. Xinjiang Geol. 20, 346–351 (in Chinese with English abstract).
Li, X.H., Liu, D.Y., Sun, M., Li, W.X., Liang, X.R., Liu, Y., 2004. Precise Sm–Nd and U-Pb isotopic dating of the supergiant Shizhuyuan polymetallic deposit and its host granite, Southeast China. Geol. Mag. 141, 225–231. https://doi.org/10.1017/S0016756803008823.
Li, X., Li, Z.X., Ge, W.C., Zhou, H.W., Li, W.X., Liu, Y., Wingate, M.T.D., 2003. Neoproterozoic granitoids in South China: crustal melting above a mantle plume at ca. 825 Ma. Precambr. Res. 122, 45–83. https://doi.org/10.1016/S0301-9268(02)00207-3.
Li, X.H., 2020. The major driving force triggering breakup of supercontinent-mantle plumes or deep subduction? Acta Geol. Sinica 94, 1–26. http://kns.cnki.net/kcms/detail/11.1951.P.20201010.1538.002.html. (in Chinese with English abstract).
Li, X.H., Li, W.X., Li, Z.H., 2007a. On the genetic classification and tectonic implications of the Early Yanshanian granitoids in the Nanling Range, South China. Chin. Sci. Bull. 52, 1873–1885. https://doi.org/10.1007/s11434-007-0259-0.
Li, X.H., Li, Z.X., Li, W.X., Liu, Y., Yuan, C., Wei, G.J., Qi, C.S., 2007b. U-Pb zircon, geochemical and Sr–Nd–Hf isotopic constraints on age and origin of Jurassic I- and A-type granites from central Guangdong, SE China: a major igneous event in response to foundering of a subducted flat-slab. Lithos 96, 186–204. https://doi.org/10.1016/j.lithos.2006.09.018.
Li, X.H., Li, Z.X., Wingate, M.T.D., Chung, S.L., Liu, Y., Lin, G.C., Li, W.X., 2006. Geochemistry of the 755 Ma Mundine Well dyke swarm, northwestern Australia: part of a Neoproterozoic mantle superplume beneath Rodinia. Precambr. Res. 146 (1–2), 1–15. https://doi.org/10.1016/j.precamres.2005.12.007.
Li, X.H., Zhou, H., Chung, S.L., Lo, C.H., Wei, G., Liu, Y., Lee, C.Y., 2002b. Geochemical and Sr–Nd isotopic characteristics of late Paleogene ultrapotassic magmatism in southeastern Tibet. Int. Geol. Rev. 44, 559–574. https://doi.org/10.2747/0020-6814.44.6.559.
Li, Z.X., Zhong, S.J., 2009. Supercontinent–superplume coupling, true polar wander and plume mobility: plate dominance in whole-mantle tectonics: Phys. Earth Planet. Inter. 176 (3–4), 143–156. https://doi.org/10.1016/j.pepi.2009.05.004.
Li, Z.X., Li, X.H., Li, W.X., Ding, S.J., 2008. Was Cathaysia part of Proterozoic Laurentia? New data from Hainan Island, south China. Terra Nova 20 (2), 154–164. https://doi.org/10.1111/j.1365-3121.2008.00802.x.
Li, Z.X., Li, X.H., Zhou, H.W., Kinny, P.D., 2002c. Grenvillian continental collision in south China: new SHRIMP U-Pb zircon results and implications for the configuration

of Rodinia. Geology 30, 163–166. https://doi.org/10.1130/0091-7613(2002)030<0163:GCCISC>2.0.CO;2.
Liu, H.Q., Xu, Y.G., Tian, W., Zhong, Y.T., Mundil, R., Li, X.H., Yang, Y.H., Luo, Z.Y., Guan, S.M., 2014a. Origin of two types of rhyolites in the Tarim Large Igneous Province: Consequences of incubation and melting of a mantle plume. Lithos 204, 59–72. https://doi.org/10.1016/j.lithos.2014.02.007.
Liu, X., Jahn, B.M., Zhao, Y., Liu, J., Ren, L., 2014b. Geochemistry and geochronology of Mesoproterozoic basement rocks from the Eastern Amery Ice Shelf and southwestern Prydz Bay, East Antarctica: Implications for a long-lived magmatic accretion in a continental arc. Gondwana Res. 314 (2), 508–547. https://doi.org/10.2475/02.2014.03.
Liu, X.C., Wang, W., Zhao, Y., Liu, J., Chen, H., Cui, Y.C., Song, B., 2016. Early Mesoproterozoic arc magmatism followed by early Neoproterozoic granulite facies metamorphism with a near-isobaric cooling path at Mount Brown, Princess Elizabeth Land, East Antarctica. Precambr. Res. 284, 30–48. https://doi.org/10.1016/j.precamres.2016.08.003.
Liu, Y.S., Hu, Z.C., Gao, S., Günther, D., Xu, J., Gao, C.G., Chen, H.H., 2008. In situ analysis of major and trace elements of anhydrous minerals by LA–ICP–MS without applying an internal standard. Chem. Geol. 257 (1–2), 34–43. https://doi.org/10.1016/j.chemgeo.2008.08.004.
Ludwig, K.R., 2003. User's Manual for Isoplot 3.00: a Geochronological Toolkit for Microsoft Excel. Berkeley Geochronol. Center Special Publication 4, 1–70.
Lu, G.M., Wang, W., Cawood, P.A., Ernst, R.E., Raveggi, M., Huang, S.F., Xue, E.K., 2020. Late Paleoproterozoic to early Mesoproterozoic mafic magmatism in the SW Yangtze Block: Mantle plumes associated with Nuna breakup? J. Geophys. Res. Solid Earth 125, 7. https://doi.org/10.1029/2019JB019260.
Lyons, T.W., Reinhard, C.T., Planavsky, N.J., 2014. The rise of oxygen in Earth's early ocean and atmosphere. Nature 506 (7488), 307–315. https://doi.org/10.1038/nature13068.
Macpherson, C.G., Dreher, S.T., Thirlwall, M.F., 2006. Adakites without slab melting: high pressure differentiation of island arc magma, Mindanao, the Philippines. Earth Planet. Sci. Lett. 243 (3–4), 581–593. https://doi.org/10.1016/j.epsl.2005.12.034.
Maity, B., Indares, A., 2018. The Geon 14 arc-related mafic rocks from the central Grenville Province. Can. J. Earth Sci. 55 (6), 545–570. https://doi.org/10.1139/cjes-2017-0197.
Maniar, P.D., Piccoli, P.M., 1989. Tectonic discrimination of granitoids. Geol. Soci. Am. Bull. 101, 635–643. https://doi.org/10.1130/0016-7606(1989)101<0635:tdog>2.3.co;2.
Maritati, A., Halpin, J.A., Whittaker, J.M., Daczko, N.R., 2019. Fingerprinting Proterozoic Bedrock in interior Wilkes Land. East Antarctica Sci. Rep. 9, 10192. https://doi.org/10.1038/s41598-019-46612-y.
Marschall, H.R., Hawkesworth, C.J., Leat, P.T., 2013. Mesoproterozoic subduction under the eastern edge of the Kalahari-Grunehogna Craton preceding Rodinia assembly: The Ritscherflya detrital zircon record, Ahlmannryggen (Dronning Maud Land, Antarctica). Precambr. Res. 236, 31–45. https://doi.org/10.1016/j.precamres.2013.07.006.
Marshall, E.W., Lassiter, J.C., Barnes, J.D., Luguet, A., Lissner, M., 2017. Mantle melt production during the 1.4 Ga Laurentia magmatic event: Isotopic constraints from Colorado Plateau mantle xenoliths. Geology 45, 519–522. https://doi.org/10.1130/G38891.1.
Maurice, A.E., Bakhit, B.R., Basta, F.F., Khiamy, A.A., 2013. Geochemistry of gabbros and granitoids (M- and I-types) from the Nubian Shield of Egypt: Roots of Neoproterozoic intra-oceanic island arc. Precambr. Res. 224, 397–411. https://doi.org/10.1016/j.precamres.2012.10.012.
Mckenzie, D., Jackson, J., Priestley, K., 2005. Thermal structure of oceanic and continental lithosphere. Earth Planet. Sci. Lett. 233 (3–4), 337–349. https://doi.org/10.1016/j.epsl.2005.02.005.
Meert, J.G., Pandit, M.K., Pradhan, V.R., Banks, J., Sirianni, R., Stroud, M., Newstead, B., Gifford, J., 2010. Precambrian crustal evolution of Peninsular India: A 3.0 billion year odyssey. J. Asian Earth Sci. 39 (6), 483–515. https://doi.org/10.1016/j.jseaes.2010.04.026.
Merino, E., Villaseca, C., Orejana, D., Jeffries, T., 2013. Gahnite, chrysoberyl and beryl co-occurrence as accessory minerals in a highly evolved peraluminous pluton: The Belvís de Monroy leucogranite (Cáceres, Spain). Lithos 179, 137–156. https://doi.org/10.1016/j.lithos.2013.08.004.
Middlemost, E.A.K., 1994. Naming materials in the magma igneous rock system. Earth Sci. Rev. 37, 215–224. https://doi.org/10.1016/0012-8252(94)90029-9.
Mikhalsky, E.V., Sheraton, J.W., Laiba, A.A., Beliatsky, B.V., 1996. Geochemistry and origin of Mesoproterozoic metavolcanic rocks from Fisher Massif, Prince Charles Mountains, East Antarctica. Antarct. Sci. 8, 85–104. https://doi.org/10.1017/S0954102096000120.
Miller, C.F., Mittlefehldt, D.W., 1982. Depletion of light rare-earth elements infelsic magmas. Geology 10, 129–133. https://doi.org/10.1130/0091-7613(1982)10<129:dolrei>2.0.co;2.
Morgan, W.J., 1971. Convection plumes in the lower mantle. Nature 230 (5288), 42–43. https://doi.org/10.1038/230042a0.
Motuza, G., Čečys, A., Kotov, A.B., Salnikova, E.B., 2006. The Žemaičių Naumiestis granitoids: new evidences for Mesoproterozoic magmatism in western Lithuania. GFF 128 (3), 243–254. https://doi.org/10.1080/11035890601283243.
Moucha, R., Forte, A.M., 2011. Changes in African topography driven by mantle convection. Nat. Geosci. 4 (10), 707–712. https://doi.org/10.1038/ngeo1235.
Mukherjee, I., Large, R.R., Corkrey, R., Danyushevsky, L.V., 2018. The Boring Billion, a slingshot for Complex Life and Earth. Sci. Rep. 8, 4432. https://doi.org/10.1038/s41598-018-22695-x.
Murphy, J.B., Nance, R.D., 2013. Speculation on the mechanism for the formation and breakup of supercontiments: Geosci. Front. 4, 15–194. https://doi.org/10.1016/j.gsf.2012.07.005.
Nagasawa, H., Schnetzler, C.C., 1971. Partitioning of rare Earth, alkali, and alkaline Earth elements between phenocrysts and acidic igneous magmas. Geochim. Cosmochim. Acta 35 (9), 953–968. https://doi.org/10.1016/0016-7037(71)90008-1.
Niu, Y.L., 2019. On the cause of continental breakup: A simple analysis in terms of driving mechanisms of plate tectonics and mantle plumes. J. Asian Earth Sci. In Press. https://doi.org/10.1016/j.jaesx.2019.100021.
Nordsvan, A.R., Collins, W.J., Li, Z.X., Spencer, C.J., Pourteau, A., Withnall, I.W., Betts, P.G., Volante, S., 2018. Laurentian crust in northeast Australia: implications for the assembly of the supercontinent Nuna. Geology 36, 251–254. https://doi.org/10.1130/G39980.1.
Obst, K., Hammer, J., Katzung, G., Korich, D., 2004. The Mesoproterozoic basement in the southern Baltic Sea: insights from the G 14–1 off-shore borehole. Int. J. Earth Sci. 93 (1), 1–12. https://doi.org/10.1007/s00531-003-0371-6.
Ordóñez-Calderón, J.C., Polat, A., Fryer, B.J., Gagnon, J.E., Raith, J.G., Appel, P.W.U., 2008. Evidence for HFSE and REE mobility during calc-silicate metasomatism, Mesoarchean (~3075 Ma) Ivisaartoq greenstone belt, southern West Greenland. Precambr. Res. 161 (3-4), 317–340. https://doi.org/10.1016/j.precamres.2007.09.004.
Pehrsson, S.Y., Eglington, B.M., Evans, D.A.D., Huston, D., Reddy, T.M., 2016. Metallogeny and its link to orogenic style during the Nuna supercontinent cycle. In: Li, Z.X., Evans, D.A.D., Murphy, J.B. (Eds.), Supercontinent Cycles Through Earth History. Geolo. Soci. Lon, 424. Special Publications. https://doi.org/10.1144/SP424.5.
Palin, R.M., White, R.W., Green, E.C.R., Diener, J.F.A., Powell, R., Holland, T.J.B., 2016. High-grade metamorphism and partial melting of basic and intermediate rocks. J. Metamorph. Geol. 34, 871–892. https://doi.org/10.1111/jmg.12212.
Peacock, S.M., 1996. Thermal and petrologic structure of subduction zones. Geophys. Monogr. Ser. 96, 119–133. https://doi.org/10.1029/GM096p0119.
Pearce, J.A., 2008. Geochemical fingerprinting of oceanic basalts with applications to ophiolite classification and the search for Archean oceanic crust. Lithos 100 (1–4), 14–48. https://doi.org/10.1016/j.lithos.2007.06.016.
Pearce, J.A., Peate, D.W., 1995. Tectonic implications of the composition of volcanic arc magmas. Annu. Rev. Earth Planet. Sci. 23 (1), 251–285. https://doi.org/10.1146/annurev.ea.23.050195.001343.
Pearce, J.A., Harris, N.B.W., Tindle, A.G., 1984. Trace element discrimination diagrams for the tectonic interpretation of granitic rocks. J. Petrol. 25 (4), 956–983. https://doi.org/10.1093/petrology/25.4.956.
Perez-Soba, C., Villaseca, C., 2010. Petrogenesis of highly fractionated I-type peraluminous granites: La Pedriza pluton (Spanish Central System). Geolo. Acta 8, 131–149. https://doi.org/10.1344/105.000001527 (in Chinese with English abstract).
Pertermann, M., Hirschmann, M.M., Hametner, K., Günther, D., Schmidt, M.W., 2004. Experimental determination of trace element partitioning between garnet and silica-rich liquid during anhydrous partial melting of MORB-like eclogite. Geochem. Geophys. Geosyst. 5, 5. https://doi.org/10.1029/2003GC000638.
Pisarevsky, S.A., Biswal, T.K., Wang, X., Waele, B.D., Ernst, R., Söderlund, U., Tait, J.A., Ratre, K., Singh, Y.K., Cleve, M., 2013. Palaeomagnetic, geochronological and geochemical study of Mesoproterozoic Lakhna Dykes in the Bastar Craton, India: Implications for the Mesoproterozoic supercontinent. Gondwana Res. 174, 125–143. https://doi.org/10.1016/j.lithos.2012.07.015.
Pisarevsky, S.A., Elming, S.Å., Pesonen, L.J., Li, Z.X., 2014a. Mesoproterozoic paleogeography: supercontinent and beyond. Precambr. Res. 244, 207–225. https://doi.org/10.1016/j.precamres.2013.05.014.
Pisarevsky, S.A., Michael, T.D., Li, Z.X., Wang, X.C., Tohver, E., Kirkland, C., 2014b. Age and paleomagnetism of the 1210 Ma Gnowangerup-Fraser dyke swarm, Western Australia, and implications for late Mesoproterozoic paleogeography. Precambr. Res. 246, 1–15. https://doi.org/10.1016/j.precamres.2014.02.011.
Polat, A., Hofmann, A.W., Rosing, M.T., 2002. Boninite-like volcanic rocks in the 3.7–3.8 Ga Isua greenstone belt, West Greenland: geochemical evidence for intraoceanic subduction zone processes in the early Earth. Chem. Geol. 184 (3–4), 231–254. https://doi.org/10.1016/S0009-2541(01)00363-1.
Pourteau, A., Smit, M.A., Li, Z.X., Collions, W.J., Nordsvan, A.R., Volante, S., 2018. 1.6 Ga crustal thickening along the final Nuna suture. Geology 46, 959–962. https://doi.org/10.1130/G45198.1.
Puchkov, V.N., Bogdanova, S.V., Ernst, R.E., Kozlov, V.I., Krasnobaev, A.A., Söderlund, U., Wingate, M.T.D., Postnikov, A.V., Sergeeva, N.D., 2013. The ca. 1380 Ma Mashak igneous event of the Southern Urals. Lithos 174, 109–124. https://doi.org/10.1016/j.lithos.2012.08.021.
Putirka, K.D., Perfit, M., Ryerson, F.J., Jackson, M.G., 2007. Ambient and excess mantle temperature. Olivine thermometry, and active vs passive upwelling. Chem. Geol. 241, 177–206. https://doi.org/10.1016/j.chemgeo.2007.01.014.
Richards, M.A., Jones, D.L., Duncan, R.A., Depaolo, D.J., 1991. A mantle plume initiation model for the Wrangellia flood basalt and other oceanic plateaus. Science 254, 263–267. https://doi.org/10.1126/science.254.5029.263.
Rivers, T., Corrigan, D., 2000. Convergent margin on southeastern Laurentia during the Mesoproterozoic: tectonic implication. Can. J. Earth Sci. 37, 359–383. https://doi.org/10.1139/e99-067.
Roberts, N.M.W., Slagstad, T., 2015. Continental growth and reworking on the edge of the Columbia and Rodinia supercontinents; 1.86–0.9 Ga accretionary orogeny in southwest Fennoscandia. Int. Geol. Rev. 57, 1582–1606. https://doi.org/10.1080/00206814.2014.958579.

Roberts, N.M.W., Slagstad, T., Parrish, R.R., Norry, M.J., Marker, M., Horstwood, M.S.A., 2013. Sedimentary recycling in arc magmas: geochemical and U-Pb-Hf-O constraints on the Mesoproterozoic Suldal Arc, SW Norway. Contrib. Miner. Petrol. 165 (3), 507–523. https://doi.org/10.1007/s00410-012-0820-y.
Rogers, C., Cousens, B., Ernst, R.E., Söderlund, U., 2019. Phosphorus and potassium metasomatic enrichment in the Mantle source of the c. 1450–1425 Ma Michael-Shabogamo gabbro of Eastern Laurentia. J. Petrol. 60, 57–84. https://doi.org/10.1093/petrology/egy104.
Rogers, J.J.W., Santosh, M., 2002. Configuration of Columbia, a Mesoproterozoic Supercontinent. Gondwana Res. 5 (1), 5–22. https://doi.org/10.1016/S1342-937X(05)70883-2.
Santosh, M., Maruyama, S., Yamamoto, S., 2009. The making and breaking of supercontinents: Some speculations based on superplumes, super downwelling and the role of tectosphere. Gondwana Res. 15 (3–4), 324–341. https://doi.org/10.1016/j.gr.2008.11.004.
Segal, I., Halicz, L., Platzner, I.T., 2003. Accurate isotope ratio measurements of ytterbium by multiple collection inductively coupled plasma mass spectrometry applying erbium and hafnium in an improved double external normalization procedure. J. Anal. At. Spectrom. 18, 1217–1223. https://doi.org/10.1039/B307016F.
Shalivahan, Bhattacharya, B.B., Rao, N.V.c, Maurya, V.P., 2014. Thin lithosphere-asthenosphere boundary beneath Eastern Indian Craton. Tectonophysics 612-613, 128–133. https://doi.org/10.1016/j.tecto.2013.11.036.
Shi, W.X., Liao, Q.A., Hu, Y.Q., Yang, Z.F., 2010. Characteristics of Mesoproterozoic granites and their geological significances from Middle Tianshan Block, East Tianshan district, NW China. Geol. Sci. Technol. Inf. 29, 29–37 (in Chinese with English abstract).
Sisson, T.W., Ratajeski, K., Hankins, W.B., 2005. Voluminous granitic magmas from common basaltic source. Contrib. Miner. Petrol. 148, 635–661. https://doi.org/10.1007/s00410-004-0632-9.
Skridlaitė, G., Whitehouse, M., Rimša, A., 2007. Evidence for a pulse of 1.45 Ga anorthosite–mangerite–charnockite–granite (AMCG) plutonism in Lithuania. implications for the Mesoproterozoic evolution of the East European Craton. Terra Nova 19 (4), 294–301. https://doi.org/10.1111/ter.2007.19.issue-410.1111/j.1365-3121.2007.00748.x.
Sláma, J., Košler, J., Condon, D.J., Crowley, J.L., Gerdes, A., Hanchar, J.M., Horstwood, M.S.A., Morris, G.A., Nasdala, L., Norberg, N., Schaltegger, U., Schoene, B., Tubret, M.N., Withehouse, M.L., 2008. Plešovice zircon-A new natural reference material for U-Pb and Hf isotopic microanalysis. Chem. Geol. 249, 1–35. https://doi.org/10.1016/j.chemgeo.2007.11.005.
Söderlund, U., Patchett, P.J., Vervoort, J.D., Isachsen, C.E., 2004. The ^{176}Lu decay constant determined by Lu–Hf and U-Pb isotope systematics of Precambrian mafic intrusions. Earth Planet. Sci. Lett. 219 (3–4), 311–324. https://doi.org/10.1016/S0012-821X(04)00012-3.
Spaggiari, C.V., Kirkland, C.L., Smithies, H.R., Wingate, M.T.D., Belousova, E.A., 2015. Transformation of an Archean craton margin during Proterozoic basin formation and magmatism: The Albany-Fraser Orogen, Western Australia. Precambr. Res. 266, 440–466. https://doi.org/10.1016/j.precamres.2015.05.036.
Spaggiari, C.V., Smithies, H.R., Kirkland, C.L., Wingate, M.T.D., England, R.N., Lu, Y.J., 2018. Buried but preserved: The Proterozoic Arubiddy Ophiolite, Madura Province, Western Australia. Precambr. Res. 317, 137–158. https://doi.org/10.1016/j.precamres.2018.08.025.
Stepanov, A., Mavrogenes, J.A., Meffre, S., Davidson, P., 2014. The key role of mica during igneous concentration of tantalum. Contri. Miner. Petrol. 167, 1009. https://doi.org/10.1007/s00410-014-1009-3.
Stern, R.J., 2002. Subduction zones. Rev. Geophys. 40, 3–38. https://doi.org/10.1029/2001RG000108.
Stimac, J., Hickmott, D., 1994. Trace-Element Partition-Coefficients for Ilmenite, Ortho-Pyroxene and Pyrrhotite in Rhyolite Determined by Micro-Pixe Analysis. Chem. Geol. 117, 313–330. https://doi.org/10.1016/0009-2541(94)90134-1.
Sun, S.S., McDonough, W.F., 1989. Chemical and isotopic systematics of oceanic basalts: implications for mantle composition and processes. Geol. Soci. Lon. Special Publications 42 (1), 313–345. https://doi.org/10.1144/GSL.SP.1989.042.01.19.
Tanaka, T., Togashi, S., Kamioka, H., Amakawa, H., Kagami, H., Hamamoto, T., Yuhara, M., Orihashi, Y., Yoneda, S., Shimizu, H., Kunimaru, T., Takahashi, K., Yanagi, T., Nakano, T., Fujimaki, H., Shinjo, R., Asahara, Y., Tanimizu, M., Dragusanu, C., 2000. JNdi-1: a neodymium isotopic reference in consistency with LaJolla neodymium. Chem. Geol. 168 (3–4), 279–281. https://doi.org/10.1016/S0009-2541(00)00198-4.
Tang, G.J., Chung, S.L., Hawkesworth, C.J., Cawood, P.A., Wang, Q., Wyman, D.A., Xu, Y.G., Zhao, Z.H., 2017. Short episodes of crust generation during protracted accretionary processes: Evidence from Central Asian Orogenic Belt, NW China. Earth Planet. Sci. Lett. 464, 142–154. https://doi.org/10.1016/j.epsl.2017.02.022.
Tatsumi, Y., Eggins, S., 1995. Subduction Zone Magmatism. Blackwell Science, Oxford.
Teixeira, W., Ernst, R.E., Hamilton, M.A., Lima, G., Ruiz, A.S., Geraldes, M.C., 2015. Widespread ca. 1.4 Ga intraplate magmatism and tectonics in a growing Amazonia. GFF 138, 241–254. https://doi.org/10.1080/11035897.2015.1042033.
Ulmer, P., Kaegi, R., Muntener, O., 2018. Experimentally derived intermediate to silica-rich arc magmas by fractional and equilibrium crystallization at 1.0 GPa: An evaluation of phase relationships, compositions, liquid lines of descent and oxygen fugacity. J. Petrol. 59, 11–58. https://doi.org/10.1093/petrology/egy017.
Ulmius, J., Andersson, J., Möller, C., 2015. Hallandian 1.45 Ga high-temperature metamorphism in Baltica: P-T evolution and SIMS U-Pb zircon ages of aluminous gneisses, SW Sweden. Precambr. Res. 265, 10–39. https://doi.org/10.1016/j.precamres.2015.04.004.
Upton, B.G.J., Ramo, O.T., Heaman, L.M., Blichert-Toft, J., Kalsbeek, F., Barry, T.L., Jepsen, H.F., 2005. The Mesoproterozoic Zig-Zag Dal basalts and associated intrusions of eastern North Greenland: mantle plume-lithosphere interaction. Contrib. Miner. Petrol. 149 (1), 40–56. https://doi.org/10.1007/s00410-004-0634-7.
Wan, B., Wu, F.Y., Chen, L., Zhao, L., Liang, X.F., Xiao, W.J., Zhu, R.X., 2019. Cyclical one-way continental rupture-drift in the Tethyan evolution:Subduction-driven plate tectonics. China Earth Sci. 62 (12), 2005–2016.
Wang, Q., Wyman, D.A., Li, Z.X., Bao, Z.W., Zhao, Z.H., Wang, Y.X., Jian, P., Yang, Y.H., Chen, L.H., 2010a. Petrology, geochronology and geochemistry of ca. 780 Ma A-type granites in South China: Petrogenesis and implications for crustal growth during the breakup of the supercontinent Rodinia. Precambr. Res. 178, 185–208. https://doi.org/10.1016/j.precamres.2010.02.004.
Wang, X.C., Li, X.H., Li, Z.X., Liu, Y., Yang, Y.H., 2010b. The Willouran basic province of South Australia: its relation to the Guibei large igneous province in South China and the breakup of Rodinia. Lithos 119 (3–4), 569–584.
Wang, X.D., Lv, X.B., Cao, X.F., Wang, Y.F., Liu, W., 2018. Palaeo-Mesoproterozoic magmatic and metamorphic events from the Kuluketage block, northeast Tarim Craton: Geochronology, geochemistry and implication for evolution of Columbia. Geol. J. 53, 120–138. https://doi.org/10.1002/gj.2881.
Wei, G.J., Liang, X.R., Li, X.H., Liu, Y., 2002. Precise measurement of Sr isotopic compositions of liquid and solid base using (LP) MCICP-MS. Geochimica 31, 295–305 (in Chinese with English abstract).
Weis, D., Kieffer, B., Maerschalk, C., Pretorius, W., Barling, J., 2005. High-precision Pb-Sr-Nd-Hf isotopic characterization of USGS BHVO-1 and BHVO-2 reference materials. Geochem. Geophys. Geosyst. 6, Q02002. https://doi.org/10.1029/2004GC000852.
Whalen, J.B., 1985. Geochemistry of an island-arc plutonic suite: the Uasilau-Yau Yau intrusive complex, New Britain. PNG. J. Petrol. 26 (3), 603–632. https://doi.org/10.1093/petrology/26.3.603.
Whalen, J.B., Currie, K.L., Chappell, B.W., 1987. A-type granites: Geochemical characteristics, discrimination and petrogenesis. Contri. Miner. Petrol. 95 (4), 407–419. https://doi.org/10.1007/BF00402202.
White, R., McKenzie, D., 1989. Magmatism at rift zones: The generation of volcanic continental margins and flood basalts. J. Geophys. Res. 94, 7685–7729. https://doi.org/10.1029/JB094iB06p07685.
Whitmeyer, S.J., Karlstrom, K.E., 2007. Tectonic model for the Proterozoic growth of north America. Geosphere 3, 220–259. https://doi.org/10.1130/GES00055.1.
Wu, F.Y., Liu, X.C., Ji, W.Q., Wang, J.M., Yang, L., 2017. Highly fractionated granites: Recognition and research. Sci. Chi. Earth Sci 60 (7), 1201–1219. https://doi.org/10.1007/s11430-016-5139-1.
Wu, C.Z., Santosh, M., Chen, Y.J., Samson, I.M., Lei, R.X., Dong, L.H., Qu, X., Gu, L.X., 2014. Geochronology and geochemistry of Early Mesoproterozoic meta-diabase sills from Quruqtagh in the northeastern Tarim Craton: implications for breakup of the Columbia supercontinent. Precambr. Res. 241, 29–43. https://doi.org/10.1016/j.precamres.2013.11.007.
Wu, F.Y., Jahn, B.M., Wilde, S.A., Lo, C.H., Yui, T.F., Lin, Q., Ge, W.C., Sun, D.Y., 2003. Highly fractionated I-type granites in NE China (I): Geochronology and petrogenesis. Lithos 66, 241–273. https://doi.org/10.1016/s0024-4937(02)00222-0.
Wu, F.Y., Sun, D.Y, Li, H.M, Jahn, B.M, Wilde, S., 2002. A-type granites in northeastern China: Age and geochemical constraints on their petrogenesis. Chem. Geol. 187 (1–2), 143–173. https://doi.org/10.1016/S0009-2541(02)00018-9.
Wu, F.Y., Yang, Y.H., Xie, L.W., Yang, J.H., Xu, P., 2006. Hf isotopic compositions of the standard zircons and baddeleyites used in U-Pb geochronology. Chem. Geol. 234 (1–2), 105–126. https://doi.org/10.1016/j.chemgeo.2006.05.003.
Xiao, W.J., Zhang, L.C., Qin, K.Z., Sun, S., Li, J.L., 2004. Paleozoic accretionary and collisional tectonics of the eastern Tianshan (China) Implications for the continental growth of central Asia. Am. J. Sci. 304, 370–395. https://doi.org/10.2475/ajs.304.4.370.
Xu, Y.G, Chung, S.L., Jahn, B.M, Wu, G., 2001. Petrologic and geochemical constraints on the petrogenesis of Permian-Triassic Emeishan flood basalts in southwestern China. Lithos 58 (3–4), 145–168. https://doi.org/10.1016/S0024-4937(01)00055-X.
Xu, Y.G., He, B., Luo, Z.Y., Liu, H.Q., 2013. Study on mantle plume and large igneous provinces in China: An overview and perspectives. Bull. Miner. Petrol. Geochem. 32, 25–39.
Yang, T., Moresi, L., Zhao, D.P, Sandiford, D., Whittaker, J., 2018. Cenozoic lithospheric deformation in Northeast Asia and the rapidly-aging Pacific Plate. Earth Planet. Sci. Lett. 492, 1–11.
Ye, X.T., Zhang, C.L., Santosh, M., Zhang, J., Fan, X.K., Zhang, J.J., 2016. Growth and evolution of Precambrian continental crust in the southwestern Tarim terrane: New evidence from the ca. 1.4Ga A-type granites and Paleoproterozoic intrusive complex. Precambr. Res. 275, 18–34. https://doi.org/10.1016/j.precamres.2015.12.017.
Yoshida, M., Santosh, M., 2011. Supercontinents, mantle dynamics and plate tectonics: A perspective based on conceptual vs. numerical models. Earth Sci. Rev. 105 (1–2), 1–24. https://doi.org/10.1016/j.earscirev.2010.12.002.
Yuan, Y., Zong, K.Q., Cawood, P.A., Cheng, H., Yu, Y.Y., Guo, J.L., Liu, Y.S., Hu, Z.C., Zhang, W., Li, M., 2019. Implication of Mesoproterozoic (~1.4 Ga) magmatism within microcontinents along the southern Central Asian Orogenic Belt. Precambr. Res. 327, 314–326. https://doi.org/10.1016/j.precamres.2019.03.014.
Zhang, K., Zhu, X.K., Wood, R.A., Shi, Y., Gao, Z.F., Poulton, S.W., 2018a. Oxygenation of the Mesoproterozoic ocean and the evolution of complex eukaryotes. Nat. Geosci. 11, 345–350. https://doi.org/10.1038/s41561-018-0111-y.
Zhang, N., Dang, Z., Huang, C., Li, Z.X., 2018b. The dominant driving force for supercontinent breakup: plume push or subduction retreat? Geosci. Front. 997–1007. http://creativecommons.org/licenses/by-nc-nd/4.0/.

Zhang, L., Ren, Z.Y., Xia, X.P., Li, J., Zhang, Z.F., 2015a. Isotope Maker: A Matlab program for isotopic data reduction. Int. J. Mass Spectrom. 392, 118–124. https://doi.org/10.1016/j.ijms.2015.09.019.

Zhang, L.M., Wang, Y.J., Qian, X., Zhang, Y.Z., He, H.Y., Zhang, A.M., 2018c. Petrogenesis of Mesoproterozoic mafc rocks in Hainan (South China) and its implication on the Southwest Hainan-Laurentia-Australia connection. Precambr. Res. 313, 119–133. https://doi.org/10.1016/j.precamres.2018.05.002.

Zhang, L.M., Zhang, Y.Z., Xiang, Cui, Cawood, P.A., Wang, Y.J., Zhang, A.M., 2019a. Mesoproterozoic rift setting of SW Hainan: Evidence from the gneissic granites and metasedimentary rocks. Precambr. Res. 325, 69–87. https://doi.org/10.1016/j.precamres.2019.02.013.

Zhang, S.C., Wang, X.M., Wang, H.J., Bjerrum, C.J., Hammarlund, E.U., Haxen, E.R., Wen, H.J., Ye, Y.T., Canfield, D.E., 2019b. Paleoenvironmental proxies and what the Xiamaling Formation tells us about the mid-Proterozoic ocean. Geobiology 17, 225–246. https://doi.org/10.1111/gbi.12337.

Zhang, S.H., Zhao, Y., Yang, Z.Y., He, Z.F., Wu, H., 2009. The 1.35 Ga diabase sills from the northern North China Craton: implications for breakup of the Columbia (Nuna) supercontinent. Earth Planet. Sci. Lett. 288 (3–4), 588–600. https://doi.org/10.1016/j.epsl.2009.10.023.

Zhang, Y.Y., Sun, M., Yuan, C., Long, X.P., Jiang, Y.D., Li, P.F., Huang, Z.Y., Du, L., 2018d. Alternating trench advance and retreat: insights from Paleozoic magmatism in the Eastern Tianshan, Central Asian Orogenic Belt. Tectonics 37, 2142–2164. https://doi.org/10.1029/2018TC005051.

Zhang, Y.Y., Sun, M., Yuan, C., Xu, Y.G., Long, X.P., Dondov, T., Wang, C.Y., He, B., 2015b. Magma mixing origin for high Ba–Sr granitic pluton in the Bayankhongor area, central Mongolia: Response to slab roll-back. J. Asian Earth Sci. 113, 353–368. https://doi.org/10.1016/j.jseaes.2014.11.029.

Zhao, G.C., He, Y.H., Sun, M., 2009. Xiong'er volcanic belt in the North China Craton: Implications for the outward accretion of the Paleo-Mesoproterozoic Columbia (Nuna) Supercontinent. Gondwana Res. 16, 170–181. https://doi.org/10.1016/j.gr.2009.02.004.

Zhao, G.C, Sun, M., Wilde, S.A., Li, S.Z., 2004. A Paleo-Mesoproterozoic supercontinent: assembly, growth and breakup. Earth Sci. Rev. 67 (1–2), 91–123. https://doi.org/10.1016/j.earscirev.2004.02.003.

Zheng, Y.F., 2019. Subduction zone geochemistry. Geosci. Fron. 10, 1223–1254. https://doi.org/10.1016/j.gsf.2019.02.003.

Zong, K.Q., Klemd, R., Yuan, Y., He, Z.Y., Guo, J.L., Shi, X.L., Liu, Y.S., Hu, Z.C., Zhang, Z.M., 2017. The assembly of Rodinia: The correlation of early Neoproterozoic (ca. 900 Ma) high-grade metamorphism and continental arc formation in the southern Beishan Orogen, southern Central Asian Orogenic Belt (CAOB). Precambr. Res. 290, 32–48. https://doi.org/10.1016/j.precamres.2016.12.010.